AN ELECTRON MICROSCOPY STUDY OF CONTINUOUS ORDERING AND PHASE SEPARATION IN IRON-RICH IRON-ALUMINUM ALLOYS

by

SAMUEL MILLER ALLEN

B.E. Stevens Institute of Technology
(1970)

S.M. Massachusetts Institute of Technology
(1971)

Submitted in partial fulfillment of the requirements

for the degree of

DOCTOR OF PHILOSOPHY

at the

Massachusetts Institute of Technology

February, 1975

Signature Redacted

Signature of Author _____
Department of Materials Science and Engineering
January 15, 1975

Signature Redacted

Certified by _____
Thesis Supervisor

Signature Redacted

Accepted by _____
Chairman, Departmental Committee on Graduate Students

ABSTRACT

AN ELECTRON MICROSCOPY STUDY OF CONTINUOUS ORDERING AND PHASE SEPARATION IN IRON-RICH IRON-ALUMINUM ALLOYS

by

SAMUEL MILLER ALLEN

Submitted to the Department of Materials Science and Engineering on January 15, 1975 in partial fulfillment of the requirements for the degree of Doctor of Philosophy.

The discrepancy between two recent phase diagram determinations of the Fe-Al system is resolved experimentally. Both diagrams are correct, but one is a metastable coherent phase diagram.

The iron-aluminum system possesses a tricritical point where a line of λ-transitions ends at a miscibility gap at about 23 atom percent aluminum and 615°C. Rules of general applicability governing phase separation within the miscibility gap are developed. Application of the rules to the iron-aluminum system results in detailed predictions about the mechanisms of decomposition and their sequences in this system. Electron microscopy is used to study the reactions experimentally and the results are in agreement with theoretical predictions.

Thesis Supervisor: John W. Cahn
Title: Professor of Metallurgy

TABLE OF CONTENTS

LIST OF ILLUSTRATIONS AND FIGURES

LIST OF TABLES

ACKNOWLEDGEMENTS

I wish to express my gratitude to all who are in some way responsible for first, making my graduate student career possible; and second, for aid in accomplishing the research which comprises this thesis.

I will always be grateful to my parents for their love and unfailing support of my educational goals. Also, my decision to attend graduate school was strongly influenced by some of the faculty at Stevens, in particular my undergraduate advisor, Steve Edelglass. I am thankful for their advice.

The financial support that I have received while at M.I.T., needless to say, has been very helpful. The Allegheny Ludlum Steel Corporation provided me with a Fellowship for two years, which I deeply appreciate. Also, the National Science Foundation's support for summer research and one academic year provided most of the funds for the research that is reported in this thesis.

Many people were involved in teaching me the experimental techniques used in this study; in particular I am grateful to Art Gregor, Bob Kelly, and many graduate students for their help in these matters. John VanderSande and Dave Laughlin were instrumental in instructing me in the use of the electron microscope.

The alloys used in this study were prepared at the General Electric Research and Development Center by Tom E. Douglas, who is to be commended for providing this brittle material in rod and sheet form.

The advice of the thesis examining committee, which consisted of Professors Morris Cohen, John VanderSande, and Dr. Philip Clapp is sincerely appreciated. Their recommendations for improvements of an initial draft were very helpful.

Valuable discussions during the course of this work were held with many people, especially John VanderSande and Sy Moss.

John Cahn's advice to me during my tenure as a graduate student has been indispensible. I particularly appreciate the freedom he always allowed me in choosing what research to work on. His insights and suggestions during the course of this thesis investigation have been invaluable. It is truly hard to imagine how a more inspiring relationship

or valuable educational experience could have been achieved other than under his tutelage.

Finally, I would like to thank my wife, Jeannie, for her love, support of my education, and helpfulness in typing the initial draft of the thesis and her assistance in preparing the figures.

I. INTRODUCTION

The existence of the ordered phases FeAl and Fe_3Al in iron-rich iron-aluminum alloys has been known for over forty years.[1] It has only been over the past twenty years that investigations have focused on determination of the phase diagram for these alloys.[2-14] Concurrently, the understanding of phase transformations in solids and the order-disorder transformation in particular has rapidly moved forward. The understanding of the order-disorder transitions in iron-rich iron-aluminum alloys in particular, however, has been rather confused as evidenced by the fact that until the past three years there has been considerable disagreement over the form of the phase diagram.[11,12] It is the conclusion of this thesis that of the recently proposed phase diagrams, two slightly different ones are correct, one being a coherent metastable phase diagram and the other the incoherent equilibrium phase diagram; also that the structures which accrue in these alloys are readily understood in terms of the types of transitions dictated by the phase diagrams and existing physical principles; furthermore, that in this system there are a wealth of phenomena which are readily adapted to test theoretical models of the behavior of solid state systems.

Bradley and Jay[1] were the first to study the order-disorder transitions in the iron-rich iron-aluminum alloys.

Their results showed that over a wide range of alloy compositions a disordered body-centered cubic phase α was stable at high temperatures, and on cooling would undergo two ordering transitions: in the first, occurring at higher temperatures, and alloy compositions from about 23 to 50 atom percent aluminum, iron and aluminum atoms take on preferred sites on the two simple cubic sublattices of the original b.c.c. crystal, with iron atoms on one sublattice and aluminum atoms on the other, resulting in a decrease of symmetry to simple cubic and a stoichiometric formula FeAl. At nonstoichiometric compositions the excess iron atoms are accomodated at random positions on the aluminum sublattice. In the second ordering transition, occurring at lower temperatures in alloys from about 22 to 40 percent aluminum, the aluminum-rich simple cubic sublattice undergoes a further ordering reaction such that the iron and aluminum atoms originally distributed at random take on preferred sites on the two face-centered cubic sublattices of the originally disordered simple cubic sublattice. This ordering transition results in a further decrease in symmetry to f.c.c. (with a unit cell whose cube edge length a_0' is twice the original b.c.c. cube edge length a_0) and a stoichiometric composition Fe_3Al.

The Strukturbericht symbols for the ordered phases FeAl and Fe_3Al are B2 and DO_3, respectively.

Since each ordering transition involves a reduction in

symmetry, superlattice reflections will appear in reciprocal space when the transitions occur. In this thesis the notation used to denote specific reflections will always refer to the 16 atom unit cell of the Fe_3Al phase. In this notation the reflections are grouped as follows: the reflections for which h, k, and l are mixed are forbidden reflections and do not occur. For (h+k+l) = 2n+1, where n is an integer, the reflections are associated with the Fe_3Al phase only. For (h+k+l) = 4n+2 the reflections are associated with both the Fe_3Al and FeAl phases. The fundamental reflections from the b.c.c. lattice are those for which (h+k+l) = 4n.

Order-disorder transitions in metals exhibit two general types of behavior near the transition temperature: The long-range order parameter can go continuously to zero as the transition temperature is approached, or it can undergo a discontinuous change at the transition temperature. Ehrenfest[15] has suggested a scheme for classifying phase changes: in a first-order transition, the first derivatives of the Gibbs free energy with respect to temperature and pressure, namely entropy and volume, have a discontinuity at the transition temperature. Such a transition necessarily has a latent heat. In a second-order transition, the entropy and volume are continuous, but the second derivatives of the Gibbs free energy with respect to temperature and pressure, i.e., heat capacity and compressibility, have discontinuities at the transition temperature. Similarly one could speak of

third-order transitions, etc. The order-disorder transitions for which the degree of long-range order is discontinuous at the transition temperature are first-order transitions. Those for which the long-range order parameter falls continuously to zero at the transition temperature are of higher than first order.

Soon after the work of Bradley and Jay, Landau[16] proposed two necessary (but not sufficient) conditions for a transition between two phases to be second-order. The first rule states that the symmetry group of the less-symmetric phase must be a subset of the symmetry group of the more-symmetric phase. In this usage a symmetry group is that set of coordinate transformations under which the "density function" $\rho(x,y,z)$ remains invariant, where $\rho(x,y,z)$ determines the probability distribution of different positions of the atoms in the crystal. The second rule requires that the number of symmetry transformations of the crystal be halved in the transition to the less-symmetric phase.

The order-disorder transitions b.c.c. $\rightarrow$ B2 and B2 $\rightarrow$ DO_3 obey the Landau rules and therefore could be second-order. As far as the phase diagram is concerned, the most obvious result of these transitions being second (or higher) order is that there would be no two-phase regions between the single-phase fields. In addition Landau showed that theoretically it would be possible for a transition to change

character; for instance at low temperatures it could be first order, and at high temperatures, second order.

In 1944, Onsager's exact solution to the two-dimensional Ising problem [17] showed that in a stoichiometric two-dimensional alloy with nearest neighbor interactions the order-disorder transition would be higher than first order. In particular, the heat capacity would rise to infinity at the transition temperature, but $\int c_p dT$ would be finite; i.e., there would be no latent heat. This transition defies classification by the Ehrenfest scheme, except to say that it is not a first order transition.

Because of this fact, and because of the shape of the c_p vs. T curve, these transitions are referred to as λ - transitions. This same type of behavior of the specific heat near the critical temperature has been observed in alloys in which the degree of long-range order decreases continuously to zero at the critical temperature. Hence the nomenclature we will adopt is that order-disorder transitions in alloys are either first-order or λ-transitions.

Experimentally it is difficult to determine unequivocally that a transition is a λ-transition.[18] Therefore early investigations of the iron-aluminum phase diagram have led to conflicting results with regard to the order of the transitions.

Developments in the field of critical phenomena, in

particular with regard to critical exponents and their measurement for the $Fe_3Al \rightarrow FeAl$ transition [19], along with a novel electron microscopy investigation[20,12] and independent X-ray diffraction studies of phase relationships in iron-aluminum alloys[11,13] are conclusive evidence that the order-disorder transitions $B2 \rightarrow DO_3$ and b.c.c. $\rightarrow$ B2 can occur by λ-transitions. In addition, the electron microscopy investigations of Swann, Duff, and Fisher[9,12] and the X-ray diffraction results of Okamoto and Beck[11] are in substantial agreement as far as the form of the phase diagram is concerned.

The currently accepted phase diagram, Figure I.1, is of great interest because of the unusual and in fact remarkable features it displays. There are two ordered phases, higher order transitions and a miscibility gap. In particular, the transition between the disordered phase α and the ordered phase FeAl changes character: at high temperatures it occurs by higher-order transition with no miscibility gap between the phases, and at lower temperatures the transition between the same phases is first-order with a miscibility gap. The point where the transition changes character is called a tricritical point.[21] Tricritical points and the transitions that occur in their vicinity are of great current interest [22] although no such point has received detailed study in an ordering alloy system.

Tricritical points occur in phase diagrams where

three lines of critical points meet. In two-component systems, these three critical curves are best seen when the phase diagram is plotted in a space of thermodynamic "fields."[21] In this sense, a "field" is an intensive thermodynamic quantity having the property that in a system at equilibrium, the "fields" are uniform at every point in the system. Thus temperature and chemical potential are "fields" in this sense. The tricritical point in the iron-aluminum phase diagram is evident when the phase diagram is plotted using the fields T, $\Delta = \mu_{Fe} - \mu_{Al}$, and η, where T is the temperature, μ_{Fe} and μ_{Al} are the chemical potentials of iron and aluminum, respectively, and η is an experimentally inaccessible "field" conjugate to the long-range order parameter, s.

The phase diagram in the immediate vicinity of the tricritical point is shown schematically in Figure I.2, analogous to that given for the He^3-He^4 system by Griffiths[21]. The entire T-Δ-η space is accessible: the Gibbs phase rule dictates that a single phase has three degrees of freedom, two phases have two degrees of freedom, and three phases have one degree of freedom. Surface I, lying in the η=0 plane, is a coexistance surface on which the long-range order parameter s is non-zero and has a positive or negative sign depending on whether $\eta \to 0$ through positive or negative values (this distinguishes between the ordered phase and its antiphase). Above the temperature T*, surface I terminates in a line of

critical points (λ-transitions, λ in Figure I.2) where the ordered phase and its antiphase become identical with the disordered phase. Below the temperature T*, surface I terminates in a decomposition curve (d in Figure I.2) where the ordered phase, its antiphase, and the disordered phase coexist.

The surface I is connected along line d to two coexistance surfaces, II and II' in Figure I.2, which extend symmetrically into the regions $\eta>0$ and $\eta<0$, and which themselves terminate in lines of critical points, shown in Figure I.2 as dashed lines. These two critical lines join the line λ at the same point as line d; hence three critical curves meet at the point P and Griffiths[21] proposed the name tricritical point for such a point.

The higher-order transitions that occur in iron-aluminum alloys have been studied by X-ray diffraction and electron microscopy. The microscopy results indicate that within a few degrees Celsius of the transition temperature fluctuations analogous to critical opalescense in liquid-liquid and liquid-vapor systems occur and in fact can be quenched in and observed at ambient temperatures in the electron microscope. Theoretical treatment of fluctuation theory in the vicinity of higher-order transitions and tricritical points[23] like that in the Fe-Al system indicates that fluctuations occur in the degree of long-range order and composition but that the

character of the fluctuations changes depending on the proximity to the tricritical point.

The miscibility gap in the phase diagram is also of interest. Simple theoretical models of binary alloys with first and second neighbor interactions have been shown in the Bragg-Williams approximation[24] to lead to equilibrium phase diagrams exhibiting features remarkably like that observed in the iron-aluminum system. The only thermodynamic investigation into the metastable possibilities for a disordered b.c.c. alloy has shown[25] that for certain values of the interaction energies the equilibrium two-phase state will be attained by first continuous ordering (by higher-order transition) and then phase separation by spinodal decomposition.

The studies of the phase diagram for iron-aluminum alloys which have used electron microscopy reveal a surprising variety of microstructure and in particular two-phase morphologies. Alloys of 10-20 atom percent aluminum, when quenched and aged, exhibit anamolous property changes known as the "K-state."[26] Electron microscopy studies attribute these phenomena to the formation of very small ($\sim$50Å diameter) Fe_3Al particles in a disordered matrix.[27,28] For alloys of higher aluminum content, closer to the tricritical composition, electron microscopy studies have shown a great variety of microstructural possibilities.[9,12,20] Since the investigations have largely focused on determining the equilibrium

phases, specimens were held a long time at temperature and little information was revealed about the mechanisms and underlying principles governing the evolution of microstructure in these alloys.

This thesis is devoted to an electron microscopy study of transformations that occur in the iron-aluminum alloys that are close to the tricritical composition. Particular emphasis is placed on the principles which govern microstructural changes in this system where higher-order transitions are a significant feature of the phase diagram.

REFERENCES

1. A.J. Bradley and A.H. Jay, Proc. Roy. Soc. London A136, 210(1932).

2. A. Taylor and R.M. Jones, J. Phys. Chem. Solids 6, 16(1958).

3. H.J. McQueen and G.C. Kuczynski, Trans. TMS-AIME 215, 619(1959).

4. P.S. Rudman, Acta Met. 8, 321(1960).

5. F. Lihl and H. Ebel, Arch. Eisenheuttenw. 7, 483(1961).

6. A. Lawley and R.W. Cahn, J. Phys. Chem. Solids 20, 204(1961).

7. L. Rimlinger, Mem. Sci. Rev. Met. 64, 847(1967).

8. J.E. Epperson and J.E. Spruiell, J. Phys. Chem. Solids 30, 1721(1969).

9. P.R. Swann, W.R. Duff, and R.M. Fisher, Trans. TMS-AIME 245, 851(1969).

10. H. Warlimont, Z. Metallk. 60, 195(1969).

11. H. Okamoto and P.A. Beck, Met. Trans. 2, 569(1971).

12. P.R. Swann, W.R. Duff, and R.M. Fisher, Met. Trans. 3, 409(1972).

13. K. Oki, M. Hasaka, and T. Eguchi, Trans. JIM 14, 8(1973).

14. K. Oki, M. Hasaka, and T. Eguchi, Jap. J. Appl. Phys. 12, 1522(1973).

15. P. Ehrenfest, Communication Leiden, Suppl. 756(1933). See discussion in: Epstein, Thermodynamics, p. 128-133, (New York, Wiley, 1937).

16. L.D. Landau and E.M. Lifshitz, Statistical Physics, p. 439, (London, Pergamon Press, 1958).

17. L. Onsager, Phys. Rev. 65, 117(1944).

18. L. Guttman, Solid State Physics 3, 145(1956).

19. L. Guttman, H.C. Schnyders, and G.J. Arai, Phys. Rev. Lett. 22, 517(1969).

20. P.R. Swann, W.R. Duff, and R.M. Fisher, Phys. Stat. Sol. 37, 577(1970).

21. R.B. Griffiths and J.C. Wheeler, Phys. Rev. A 2, 1047(1970).

22. Physics Today 27(5), 17(1974).

23. M.A. Krivoglaz, Theory of X-Ray and Thermal Neutron Scattering by Real Crystals, Plenum Publishing Corp. (1969).

24. G. Inden, Acta. Met., 22, 945 (1974).

25. M.J. Richards, Sc. D. Thesis, MIT, Cambridge, Mass. (1971).

26. H. Thomas, Z. Physik 129, 219(1951).

27. H. Warlimont and G. Thomas, Metal Sci. Jour. 4, 47(1970).

28. D. Watanabe, J. Phys. Soc. Japan 29, 722(1970).

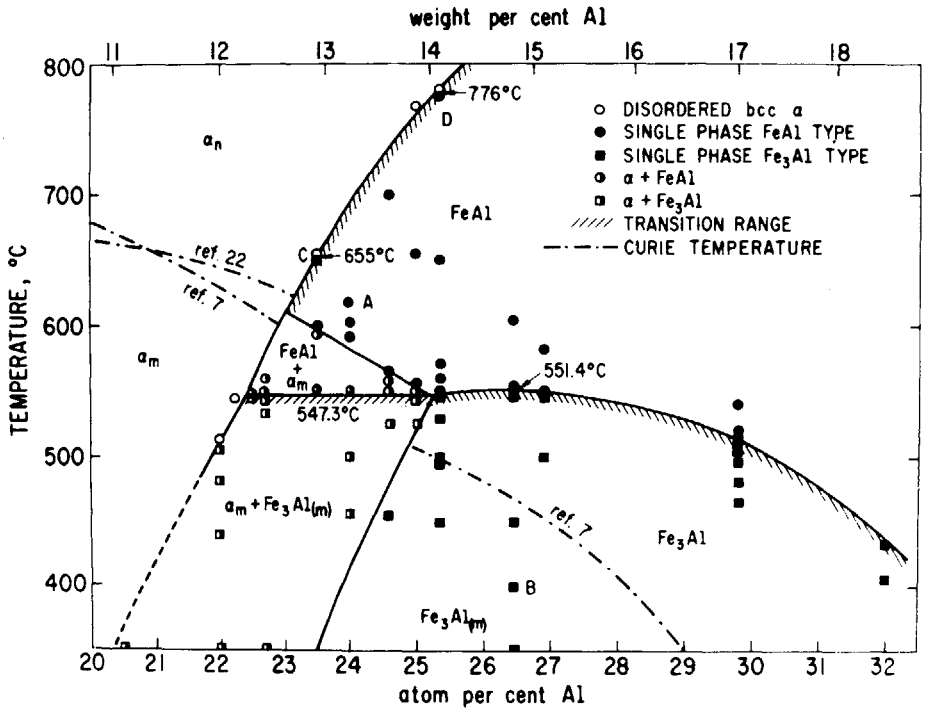

Figure I.1

The Iron-Aluminum Phase diagram as determined by the electron microscopy studies of Swann, Duff, and Fisher (References 9 and 12).

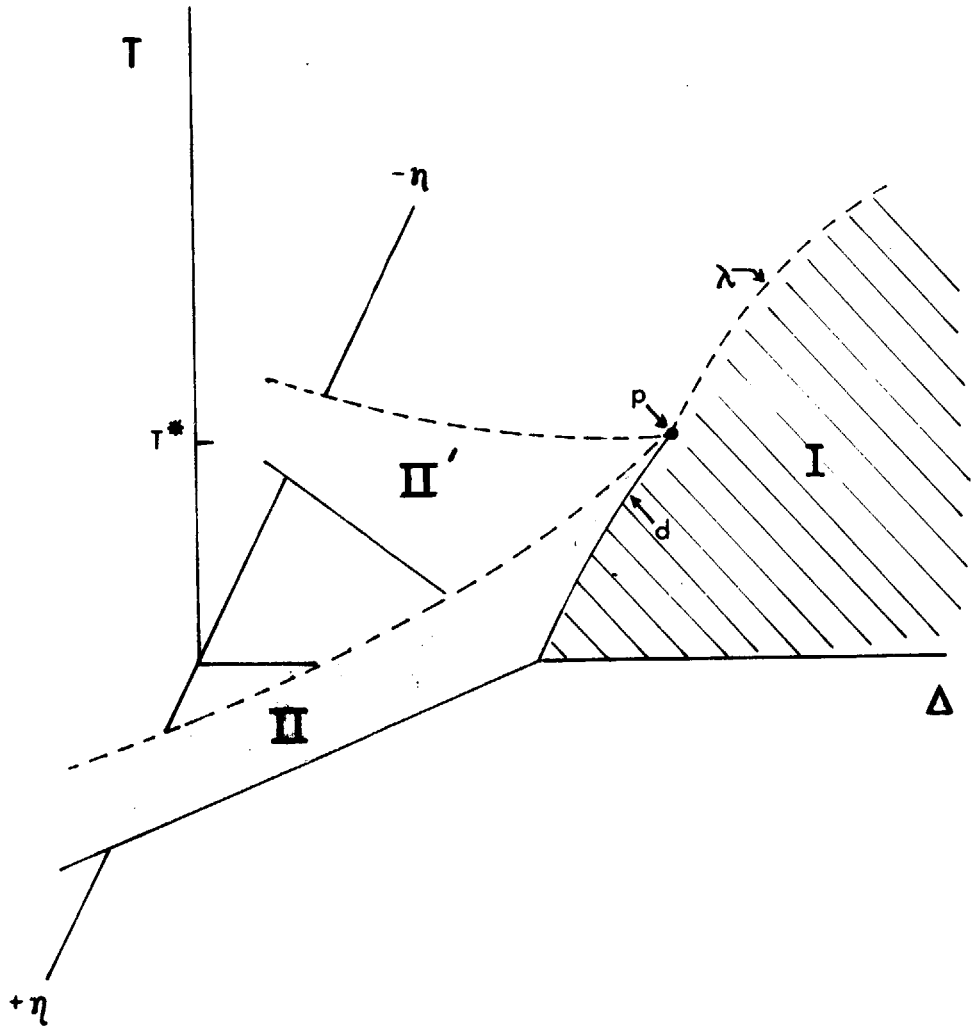

Figure I.2

A schematic representation of the iron-aluminum phase diagram in the immediate vicinity of the tricritical point P, plotted in the space of thermodynamic fields T, Δ and η, where T is the temperature, Δ is the chemical potential difference between iron and aluminum atoms, and η is an experimentally inaccessible field conjugate to the long range order parameter. Each of the coexistance surfaces I, II and II' terminates in a line of critical points (broken curves), all of which intersect at the tricritical point.

II. ON THE EXISTENCE OF COHERENT AND INCOHERENT PHASE DIAGRAMS FOR IRON-RICH IRON-ALUMINUM ALLOYS

Abstract

The discrepancy between two recent phase diagram determinations of the Fe-Al system is resolved experimentally. Both diagrams are correct, but one is a metastable coherent phase diagram.

II.1 Introduction

The ordered phases FeAl and Fe_3Al were first discovered in iron-rich iron-aluminum alloys more than forty years ago.[1] Since then, many different phase diagrams have been proposed for these alloys[2-14] and it was not until the past five years that there has been significant qualitative agreement concerning the form of the phase diagram detween separate investigations using complementary techniques.

Figure II.1 is a superposition of two recent determinations of the phase diagram for iron-aluminum alloys; those due to the electron microscopy study of Swann, Duff and Fisher[9,12] (SDF), and to the X-ray diffraction study of Okamoto and Beck[11] (OB). Both diagrams have two lines of λ-transitions: one between the disordered phase α and the FeAl phase which ends at a miscibility gap between the same phases, and another between the FeAl and Fe_3Al phases which terminates at a two-phase field. Hence, detailed independent

investigations, using different techniques, have arrived at phase diagrams with essentially the same qualitative features, features that are very unusual in metallurgical systems.

There are significant differences between the SDF and OB phase diagrams apparent in Figure II.1; namely the extent of the two-phase fields α + FeAl and α + Fe_3Al. In these alloys accurate chemical analysis is difficult; this could explain small discrepancies between the two diagrams. The fact that the OB study determined the maximum extent of the α + FeAl field to be 40°C higher than the SDF study has no immediate simple explanation. For this reason an experiment was performed to determine which was the correct phase diagram. Specimens were heat treated at points in the phase diagram where the two diagrams disagree with regard to which phases are present. Electron microscopy was used to investigate the resulting microstructure.

II.2 Experimental Procedures

The preliminary experiment described above and subsequent experiments were performed as follows:

An alloy of 23.0 atom percent aluminum was prepared at the General Electric Research and Development Center from 99.99% Fe and 99.999% Al by vacuum induction melting. Ingots were chill cast into 2.5 cm diameter molds, then hot swaged to

5 mm diameter rods. The as-received microstructure was approximately 50% recrystallized. Pieces of the rod were machined to 3 mm diameter, then given a 15 minute disordering treatment in argon at 725°C and rapidly quenched into water.

Heat treating was performed as follows:

Discs 0.25 mm thick were cut from the rod by EDM, then polished by hand to remove the spark-affected zone. The discs were then sealed in evacuated capsules. The encapsulated specimens were heat treated in a vertical furnace that was equipped for rapid quenching. Quenching was accomplished by ejecting the capsule out the bottom of the furnace into a cold brine quenchant. Submerged in the brine was a heavy metal object placed so that the capsule was broken immediately upon entering the quenchant.

In addition, one heat treatment involved a disordering treatment, followed by a lower temperature aging to produce the ordered phase, without first quenching to room temperature. For this experiment the disc specimens were wrapped in stainless steel foil and heat treated in two lead pots. Specimens were rapidly transferred by hand between the two pots and into a cold brine quenchant at the end of the aging treatment.

Electron microscopy specimens were prepared using a double jet electropolisher with an electrolyte of two parts methanol to one part nitric acid. Polishing temperature was -40 to -50°C and current densities were in the range of

0.5 - 1.5 amp/cm^2.

Electron microscopy was done at 100 KV using a JEM 7.

II.3 Results of the Key Experiment

An initially disordered and quenched iron-23.0 atom percent aluminum alloy was aged at 620°C for 4 hours and rapidly quenched. This point is near the tricritical point in the SDF diagram, and lies well below the tricritical point in the OB diagram. Figure II.2 shows a (200) dark field electron micrograph of the specimen, imaging a superlattice reflection from the FeAl phase. The bottom-most dark area of the micrograph is an out-of-contrast grain. In the adjacent grain above, a thin layer of the ordered phase FeAl has formed along the grain boundary and appears bright in this micrograph. The grain interior is also single-phase ordered FeAl, and 1/4 a'_o [111] antiphase boundaries are visible as dark lines within the ordered phase.[15] Separating the FeAl grain boundary layer from the grain interior is a layer which appears dark in this micrograph. Dark-field microscopy using a fundamental reflection reveals that this layer is disordered α with approximately the same orientation as the adjoining FeAl phases.

The most reasonable interpretation of this result leads to the following hypothesis which will be proven in the remainder of the paper.

II.4 Coherency Hypothesis

Neglecting small errors in chemical analysis, both the SDF and OB phase diagrams are correct. The OB phase diagram is the equilibrium incoherent diagram, while the SDF diagram is a coherent metastable phase diagram for these alloys.

Thus, if the hypothesis is correct, two phases that lie along the grain boundary in Figure II.2 are equilibrium incoherent phases reported by OB for this temperature. The phase in the grain interior is that seen by SDF and represents coherent phase equilibrium.[16,17]

II.5 Requirements for Proof of the Hypothesis

Experimental verification of the hypothesis requires that each phase diagram represent reversible equilibria, and that the following requirements are met:

1. At points where the two diagrams differ with respect to the number of equilibrium phases, and the observed microstructure lacks one of the predicted phases, it must be shown that nucleation or other kinetic barriers (except for loss of coherency) did not prevent the formation of the missing phase.

2. The coherent phases must be in metastable equilibrium and must be unstable in the presence of the incoherent phases.

3. Coherency strains must be present in the coherent

multi-phase structure and dislocations must be visible in the interfaces between the incoherent phases eliminating (or reducing) coherency strains.

4. It must be shown that the grain boundary phases are not the result of contamination with elements other than iron and aluminum, such as oxygen and carbon.

II.6 Results

This section is a presentation of our results which demonstrate the truth of each of the above points and hence together confirm the hypothesis.

The following results pertain to the observations of structures developed in the key experiment. In that experiment the specimen was disordered and quenched, then reheated to 620°C, held there for four hours, and quenched. Electron microscopy of specimens that were quenched from the disordered region of the phase diagram to room temperature shows that FeAl ordering is not supressed, but that some α phase is retained. If indeed the microstructure shown in Figure II.2 developed from an initial state at 620°C which contained some α phase, it would be significant; for this would mean that no kinetic barrier to the formation of coherent α can explain its absence in the bulk of the microstructure, and that the disordered α phase was unstable with respect to formation of single-phase FeAl. Because it was not possible to know if any

α would be retained during heating to 620°C in the key experiment, the following experiment was performed: A specimen was disordered at 675°C, then plunged into molten lead at 620°C, held there for four hours, then quenched to room temperature. The resulting microstructure was single-phase FeAl, identical to that observed in the bulk of the specimen shown in Figure II.2. Thus there is conclusive evidence that α is unstable with respect to the formation of single-phase FeAl at 620°C.

Thus we have established that the SDF diagram is correct within the accuracy of chemical analysis at 620°C and 23 a/o Al in predicting that single-phase FeAl is stable with respect to the presence of coherent α or single-phase α of the same composition. Furthermore it is our experience[18] that coherent equilibria are reached well within the times allotted by SDF and we have found no evidence that is inconsistent with any other part of the SDF diagram.

Our own electron microscopy observations of Fe-23% Al specimens held at 570°C and 530°C (within the two-phase regions of both the SDF and OB phase diagrams) for times ranging from 20 minutes to 1100 minutes have shown that the grain boundary phases are absent at short aging times, and are observed most frequently at long aging times, although not on all grain boundaries. At each heat treatment temperature the thickest layers of phases observed at the grain boundary were observed for the specimens heat treated the longest. Thus, our conclusion is that nucleation of the grain boundary phases is not

easy and only occurs at isolated points, and that the volume fraction of the grain boundary phases increases with time. We conclude, therefore, that the coherent phases are indeed metastable, but unstable in the presence of the grain boundary phases.

Figure II.3 is a dark-field electron micrograph of a Fe-23% Al alloy, initially disordered, quenched, and then aged at 530°C for 1110 minutes at a point within the α + Fe_3Al region of both the SDF and OB phase diagrams. The microstructure in the vicinity of a three-grain junction is shown by imaging (111) and (200) superlattice reflections from the lower and upper grains, respectively. The grain in the upper right corner of the micrograph is out of contrast and appears dark. A layer of the Fe_3Al phase has formed within the lower grain along the grain boundary, separated from the grain interiors by layers of the disordered phase. The grain interiors are two-phase α + Fe_3Al also, with a high degree of connectivity within the ordered phase.

Bright-field microscopy was used to investigate the nature of the interface between the ordered and disordered grain boundary phases in this specimen. Figure II.4 shows a bright-field electron micrograph of this interface. Dislocations are visible in the interface and in addition antiphase boundaries are visible in the Fe_3Al grain boundary layer because of the strongly diffracting superlattice reflections.

Antiphase boundaries result from dislocation motion in these alloys, and because the antiphase boundaries visible in Figure II.4 are rather straight, it is reasonable to expect that they formed as a result of dislocations moving out of the grain boundary and into the interface between the incoherent phases, aiding in the reduction of coherency strains. The fact that dislocations are not usually seen at the points where the antiphase boundaries intersect the boundary between the incoherent phases can be explained as follows: On reaching the boundary, the dislocations began to slip in the plane of the interface toward the lowest energy configuration. A self consistent model can be developed to support this argument taking into account the observed slip plane traces, their apparent width, and assuming that slip plane occurs on {110} planes with Burgers vectors of the type 1/4 a'_o [111].

The antiphase boundary morphology in the bulk FeAl phase in Figure II.2 is remarkable because there is an apparent anisotropy to the antiphase boundary structure which has not been observed in other studies of FeAl.[12,15] A reasonable explanation is that the straight portions of antiphase boundary are the result of dislocation motion occurring near the grain boundary during the heat treatment to alleviate coherency strains caused by the formation of the equilibrium phases at the grain boundary. Some of these dislocations are located at terminations of antiphase boundaries. Where a

dislocation crossed an existing boundary the crossing is unstable. It dissociated into two approximately hyperbolic sheets[19] by diffusional motion of the boundaries driven by reduction in boundary area. This has occurred in Figure II.2 and shows that dislocation motion occurred slowly at high temperatures.

Figure II.2 shows the composition difference between the FeAl phase in the bulk of the grain and the FeAl phase at the grain boundary. The mottled background and the associated broadening of antiphase boundaries in the bulk FeAl phase has been demonstrated by Swann, Duff and Fisher[12,20] to be due to critical point fluctuations associated with proximity to the line of λ-transitions, and not the presence of a second phase. The composition of this specimen was very close to the composition where the line of λ-transitions for the reaction $\alpha \rightarrow$ FeAl ends in a miscibility gap. In accordance with current terminology in the physics literature, we refer hereafter to this point as a tricritical point.[21] Near the tricritical point fluctuations are present not only in the degree of long-range order but also in composition.[22] This gives rise to the fine scale background in Figure II.2, because the specimen was heat treated very close to the tricritical point in the SDF phase diagram. The FeAl layer formed at the grain boundary does not show the fluctuations, indicating that in accord with the OB diagram its composition

is removed from the tricritical composition and is therefore different from the composition of the FeAl phase in the bulk of the grain.

With regard to the possibility of contaminants at the grain boundaries causing the formation of some unknown phase, the following points are made:

In selected-area diffraction, the reflections from the boundary phases coincide with those of α, FeAl, and Fe_3Al. The ordered boundary phase always showed the expected domain structure of either FeAl or Fe_3Al, depending upon temperature in accord with the OB diagram. Furthermore, the ASTM index of powder diffraction lines lists no known compounds of iron or aluminum with carbon, oxygen, or anything else having these lattice parameters.

II.7 Discussion

Taken together, the results represent experimental proof of the hypothesis: namely, that the OB phase diagram is the equilibrium incoherent phase diagram, and that the SDF phase diagram is the coherent metastable diagram. The differences in techniques of the OB and SDF studies are compatible with this result. In the OB study, filings were made from homogenized ingots, then heat treated at one temperature for times ranging from a few days to a few weeks, depending on the temperature. The deformation induced by filing, coupled

with the small particle size and long heat treatment times could have contributed to coherency loss and formation of the stable equilibrium phases.

In contrast, the SDF study used sheet specimens which had received a homogenization treatment at 1000°C prior to final heat treating for their phase diagram study. Heat treatment times in the SDF study were in the range of several minutes to a few days, depending on the temperature.

In the present study, the as-received microstructure was approximately 50% recrystallized, and heat treating was performed on material in this condition. Thus the presence of some grains with high dislocation density would have aided the formation of the equilibrium phases.

Besides the OB and SDF phase diagrams, others have been proposed in recent years. The diagram of Oki, Hasaka, and Eguchi[13,14] (OHE) is very similar to the SDF phase diagram except for a major systematic composition shift, possibly due to a systematic error in chemical analysis. The phase diagram by Warlimont[10] differs from those of SDF, OB and OHE in the respect that it lacks the lines of λ-transitions and consequently the tricritical point, possibly due to misinterpretation of the critical fluctuations near the lines of λ-transitions. Our own study has not dealt with the FeAl → Fe_3Al transition in detail, but we concur with SDF that the α → FeAl transition is not first order above the tri-

critical composition.

Now that both the SDF and OB phase diagrams have been shown to apply to these alloys, a composite incoherent/coherent phase diagram may be inferred, based on these studies and rigorous thermodynamic principles. The relative positions of the phase boundaries in the temperature-composition plane will be established first, then consideration of slope changes in the phase boundaries will be dealt with.

The coherent phase diagram is metastable and the incoherent phase diagram is stable. Since thermodynamics dictates that the extent of a single-phase domain on a phase diagram is always expanded when it is metastable, in this instance the two-phase regions of the coherent phase diagram must lie within the two-phase regions of the incoherent diagram. Since λ-transitions occur continuously with no nucleation barrier, the critical curves for the λ transitions in the coherent and incoherent phase diagrams must be coincident. Thermodynamics also demands that the parts of the critical curves for the λ-transitions $\alpha \rightarrow$ FeAl and FeAl $\rightarrow$ Fe_3Al in the coherent diagram which lie within the equilibrium two-phase fields must be metastable extensions of the equilibrium critical curves for the same transitions.

Figure II.5 shows the form of the coherent/incoherent diagram drawn with regard to the above rules. The position of the phase boundaries with respect to the temperature-

composition axes is based on the following: In both the OB study and the present one the reported alloy compositions are upper bounds to the actual compositions, since aluminum is easily lost from the molten alloy by oxidation. On the other hand, the alloys studied by SDF were chemically analyzed, and the position of the $\alpha \rightarrow$ FeAl critical curve according to SDF is in close agreement with the x-ray study of Lawley and Cahn[16] who claim an accuracy of 0.2 atom percent in analysis of their own alloys. Since our 23 atom percent aluminum alloy was single-phase FeAl at 620°C when in coherent equilibrium, we conclude that our 23 percent alloy lies at the left end of the SDF FeAl field.

Because the SDF phase diagram represents coherent solvi, the differences in positions of phase boundaries between the SDF and OB studies give the undercoolings and supersaturations necessary for the coherent formation of new phases. A theoretical check that the observed differences are reasonable cannot be made without more specific knowledge about the variation of lattice parameter with degree of order and composition and the elastic properties of these alloys. It is reasonable to expect that in the neighborhood of a λ-transition both the lattice parameters and elastic constants will change rapidly. OB have reported a strong composition dependence of the lattice parameter of the FeAl phase in the

vicinity o f the critical composition in a series of alloys quenched after equilibrating at one temperature.

The positions of the horizontal lines separating the α + FeAl and α + Fe_3Al two-phase regions in the two phase diagrams is determined by the intersection of the line of λ-transitions for the FeAl $\rightarrow$ Fe_3Al reaction with the coherent and incoherent boundaries between the FeAl and α + FeAl regions. Therefore, since the SDF study has shown that the line of λ-transitions goes through a maximum near 26% Al, the horizontal line must be lower in the coherent diagram than in the incoherent diagram. This fact is born out in the SDF and OB studies: the position of the horizontal boundary between the α + FeAl and α + Fe_3Al two-phase regions was established as 547 $\pm$ 0.2°C in the SDF study, and at between 550°C and 555°C by the OB study.

Another requirement of thermodynamics and one which was overlooked in the OB, SDF, and OHE studies is that the slope of the phase boundary separating the α field from the two-phase fields must be continuous at its intersection with the horizontal boundary between the α + FeAl and α + Fe_3Al two-phase fields. This is a consequence of the fact that the FeAl $\rightarrow$ Fe_3Al transition is of higher than first order, and is demonstrated as follows:

The following differential equation is valid for the temperature dependence of the composition of coexisting phases

α and FeAl without any special assumptions:[23]

$$\frac{dc^{\alpha}}{dT} = \frac{(1-c^{FeAl})\Lambda_{Fe}^{\alpha\rightarrow FeAl} + c^{FeAl}\,\Lambda_{Al}^{\alpha\rightarrow FeAl}}{(c^{FeAl}-c^{\alpha})\,T\,\dfrac{\partial^2 F^{M(\alpha)}}{\partial c_{\alpha}^{2}}} \qquad (II.1)$$

where c^{α} and c^{FeAl} are the compositions of phases α and FeAl, respectively, T is the temperature, $F^{M(\alpha)}$ is the relative integral molar free energy of phase α, and $\Lambda_{Fe}^{\alpha\rightarrow FeAl}$ is the amount of heat required for the reversible transference of 1 mole of Fe from the α phase to the FeAl phase under equilibrium conditions. Likewise, $\Lambda_{Al}^{\alpha\rightarrow FeAl}$ is related to the transference of Al. The same equation is valid for the boundary to the α + Fe_3Al region of the phase diagram if Fe_3Al is substituted for FeAl in the superscripts of Equation 1. Since the FeAl → Fe_3Al transition is a λ-transition, all of the terms in Equation 1 are continuous in the vicinity of the horizontal boundary between the two two-phase regions of the phase diagram. Therefore $\frac{dc}{dT}$ is continuous in this part of the phase diagram and there can be no discontinuous change in slope of the phase boundary between the α region and the two-phase regions at the point where the horizontal boundary meets the coexistence curve. This result is true for both the incoherent and coherent phase diagrams and is incorporated in the composite coherent/incoherent phase diagram, Figure II.5, and is a correction to the SDF and OB phase diagrams. It is

important to note that the curvature of the phase boundary may be discontinuous at the point in question, since the derivative with respect to temperature of the right hand side of Equation II,1 involves the heat capacity and the heat capacity becomes infinite at a λ-transition.

A final point to consider is the slope of the phase boundary separating the disordered single-phase region from the FeAl and α + FeAl regions of the phase diagram in the vicinity of the tricritical point. Much theoretical and experimental work is in progress in the area of behavior near such a point, and some pertinent results are:

1. The classical phenomenological theory of Landau[24] can predict tricritical behavior in systems like Fe-Al. Landau asserted that there would be no slope change at the tricritical point of the boundary with the α region.

2. Experimental measurements in other systems have found tricritical points, and the phase diagrams show slope changes between the line of λ-transitions and both decomposition curves at the tricritical point.

3. The fact that the quantitative predictions of the Landau theory are not always in agreement with experiment has long been recognized.[25] In fact, Griffiths[26] has suggested that the usual discrepancies with the classical theory may all be related. He has proposed a free energy function valid near the tricritical point for He^3 -He^4 mixtures which removes the discrepancies and results in a slope change in this part

of the phase diagram.

We have chosen to draw this part of the phase diagram with a slope change because other types of systems with tricritical points seem to behave in this way. Griffiths points out, however, that there is no reason to expect that all systems with tricritical points will behave in the same way,[26] and we must conclude therefore that further research will be required to settle this point.

A further consequence of the existence of two phase diagrams, each with its own tricritical point, is that it is not likely that the coming together of two lines of λ-transitions, namely for the $\alpha \rightarrow$ FeAl ordering transition and the paramagnetic to ferromagnetic transition, is responsible for the existence of the tricritical point observed in the coherent diagram as has been suggested.[12] Recent statistical thermodynamic calculations employing the Bragg-Williams[27] as well as pair approximation have in fact predicted the tricritical behavior for b.c.c. alloys without taking into account magnetic interactions.

The existence of the two phase diagrams has a further consequence: the fluctuations observed near the tricritical point in the coherent phase diagram should be different in character from those observed near the incoherent tricritical point. A much stronger composition component to the fluctuations should be observed near the coherent tricritical point,

whereas it would be expected that at the incoherent tricritical point the fluctuations would have the same character as anywhere else along the line of λ-transitions (except in the vicinity of the coherent tricritical point).

It is important to point out that both phase diagrams are useful and either phase diagram by itself is inadequate to understand the phase behavior in the Fe-Al system. The OB diagram indeed represents stable equilibria and is without doubt all that is traditionally reported. Nevertheless, the SDF diagram represents reversible metastable equilibria that are quickly reached and are maintained for long periods of time, but of course not forever.

II.8 Conclusions

1. Two recent determinations of the iron-aluminum phase diagram containing significant differences are both valid for this system.

2. The differences in these phase diagrams are due to the fact that one is the incoherent equilibrium diagram, while the other is a coherent metastable diagram.

3. A single composite phase diagram for these alloys may be constructed consistent with both previously published diagrams employing shifts in composition that are well within the limits of errors in chemical analysis for these alloys.

4. The existence of two tricritical points, one in

the coherent and one in the incoherent phase diagrams belies the conjecture that the λ-transition for the paramagnetic to ferromagnetic change in these alloys is related to the existence of a tricritical point in the coherent phase diagram.

II.9 References

1. A.J. Bradley and A.H. Jay, Proc. Roy. Soc. London A136, 210(1932).

2. A. Taylor and R.M. Jones, J. Phys. Chem. Solids 6, 16(1958).

3. H.J. McQueen and G.C. Kuczynski, Trans. TMS-AIME 215, 619(1959).

4. P.S. Rudman, Acta Met. 8, 321(1960).

5. F. Lihl and H. Ebel, Arch. Eisenheuttenw. 7, 483(1961).

6. A. Lawley and R. W. Cahn, J. Phys. Chem. Solids 20, 204(1961).

7. L. Rimlinger, Mem. Sci. Rev. Met. 64, 847(1967).

8. J.E. Epperson and J.E. Spruiell, J. Phys. Chem. Solids 30, 1721(1969).

9. P.R. Swann, W.R. Duff, and R.M. Fisher, Trans. TMS-AIME 245, 851(1969).

10. H. Warlimont, Z. Metallk, 60, 195(1969).

11. H. Okamoto and P.A. Beck, Met. Trans. 2, 569(1971).

12. P.R. Swann, W.R. Duff, and R.M. Fisher, Met. Trans. 3, 409(1972).

13. K. Oki, M. Hasaka, and T. Eguchi, Trans. JIM 14, 8(1973).

14. K. Oki, M. Hasaka, and T. Egichi, Jap. J. Appl. Phys. 12, 1522(1973).

15. M.J. Marcinkowski and N. Brown, J. Appl. Phys. 33, 537 (1962).

16. J.W. Cahn, Acta Met. 10, 907(1962).

17. J.W. Cahn, Acta Met. 14, 83(1966).

18. Present work, Chapter III.

19. W.W. Mullins, J. Appl. Phys. 27, 900(1956).

20. P.R. Swann, W.R. Duff, and R.M. Fisher, Phys. Stat. Sol. 37, 577(1970).

21. R.B. Griffiths and J.C. Wheeler, Phys. Rev. A2, 1047 (1970).

22. M.A. Krivoglaz, Theory of X-Ray and Thermal Neutron Scattering by Real Crystals, (Plenum Publishing Corp., 1969).

23. C. Wagner, Thermodynamics of Alloys, p. 67 (Cambridge, Mass., Addison-Wesley Press, 1952).

24. L.D. Landau, Zh. Eksperim. i Teor. Fiz. 7, 19(1937), Phys. Z. Sowjetunion 11, 26(1937).

25. L. Onsager, Phys. Rev. 65, 117(1944).

26. R.B. Griffiths, Phys. Rev. Lett. 24, 71-(1970).

27. G. Inden, Acta Met., to be published.

28. R. Kikuchi and C.M. van Baal, Scripta Met. 8, 425(1974).

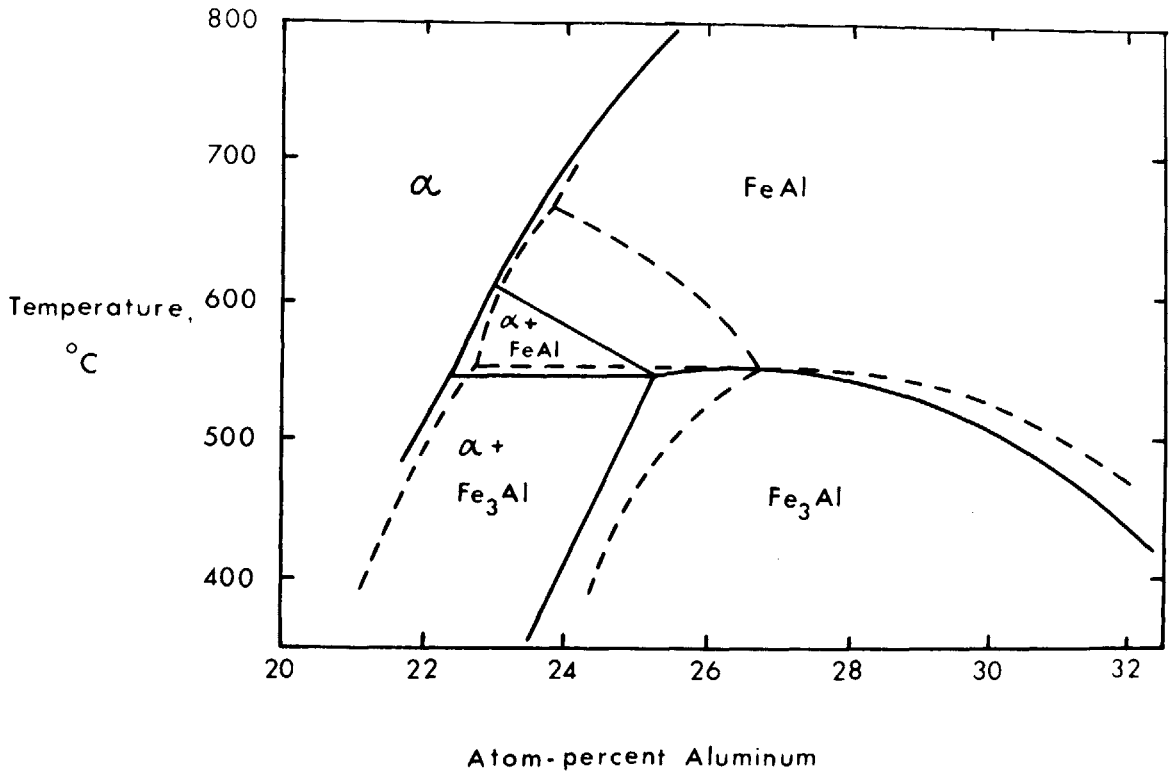

Figure II.1

The iron-aluminum phase diagram. A superposition of the diagrams of Swann, Duff, and Fisher (solid lines) and Okamoto and Beck (broken lines). From references 9, 11, and 12.

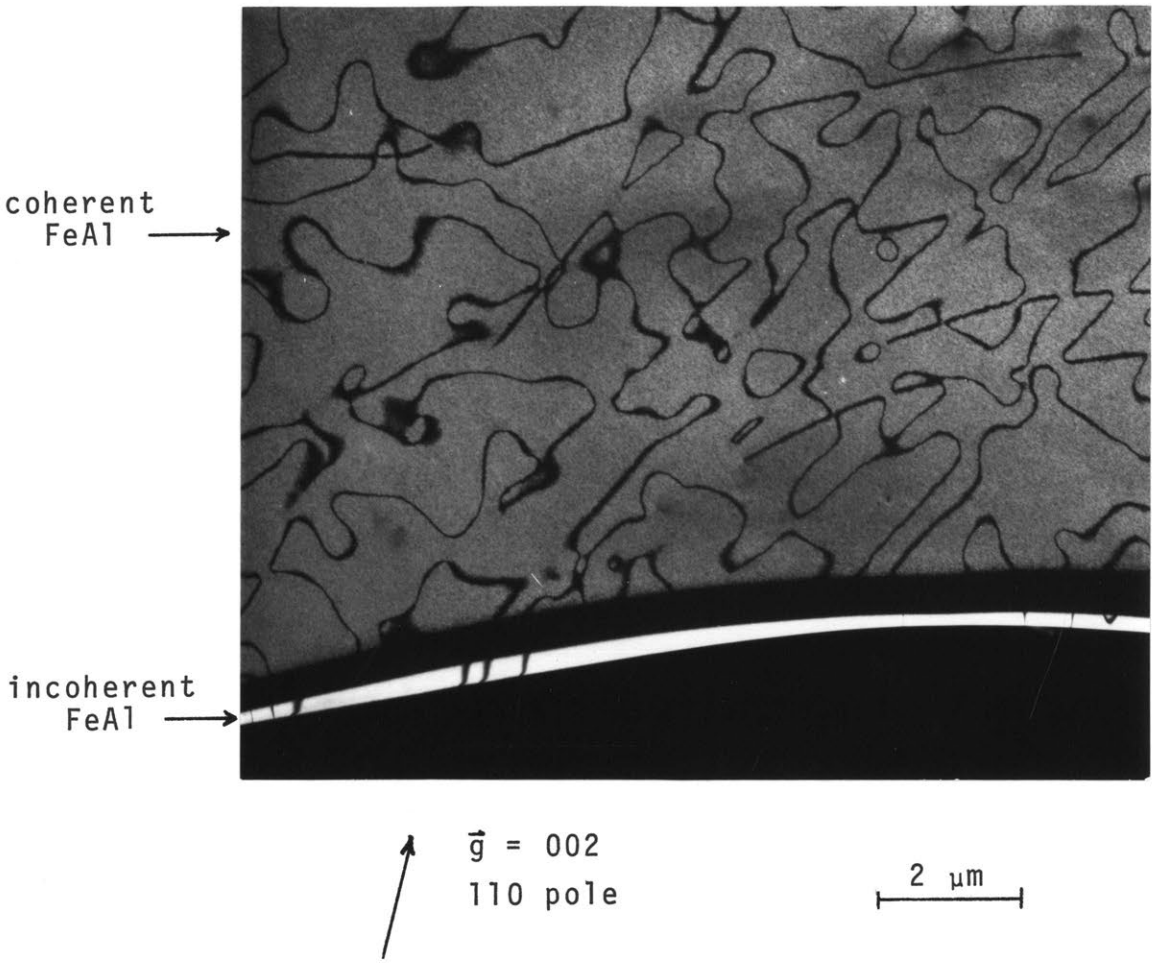

Figure II.2

A (200) dark-field micrograph of an Fe-23Al alloy, initially disordered, quenched, and aged at 620°C for 4 hours. It is the hypothesis and conclusion of this paper that the microstructure shows simultaneous attainment of two types of equilibria; single-phase ordered FeAl phase within the grain in coherent metastable equilibrium in accordance with the SDF phase diagram, and the two-phase state, α + FeAl, along the grain boundary in incoherent equilibrium in accordance with the OB phase diagram.

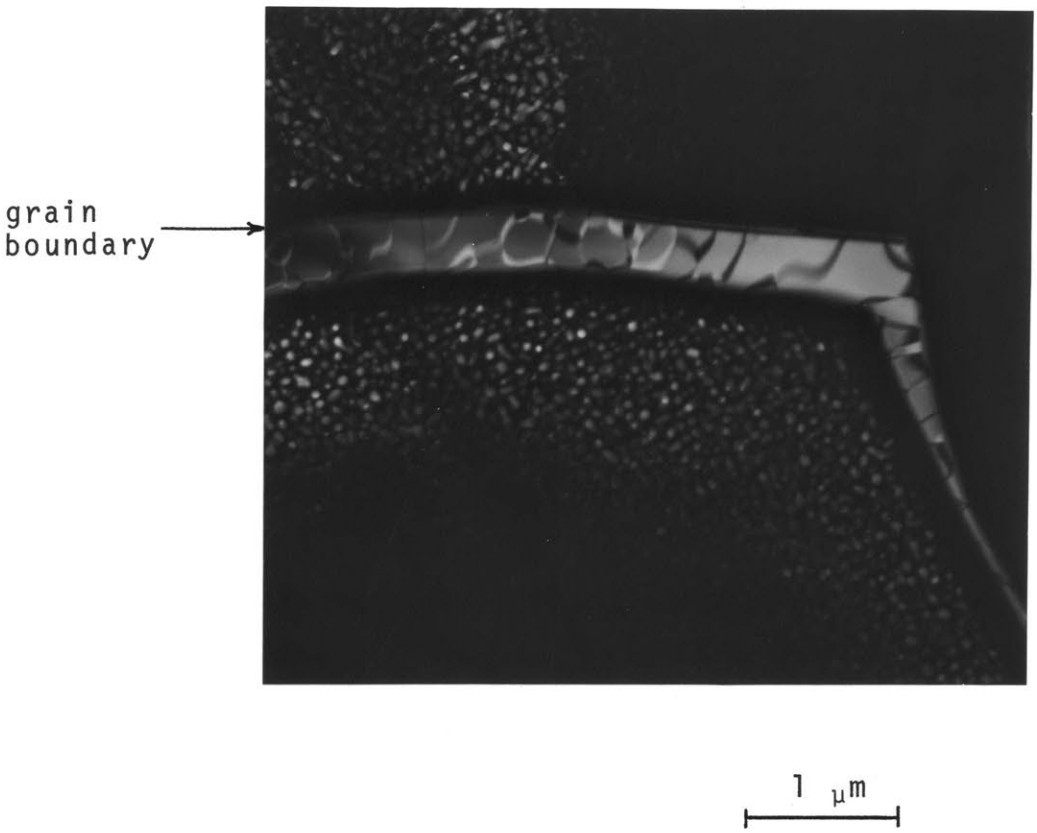

Figure II.3

An Fe-23% Al alloy, initially disordered, quenched, and aged for 1110 minutes at 530°C. A dark-field electron micrograph imaging superlattice reflections from two adjacent grains simultaneously shows the microstructure when both coherent and incoherent equilibria dictate that the equilibrium state is two-phase, α + Fe_3Al. An incoherent layer of Fe_3Al has formed on the lower side of the grain boundary. The coherent two-phase morphology within the grain interiors is separated from the Fe_3Al grain boundary layer by layers of the disordered phase.

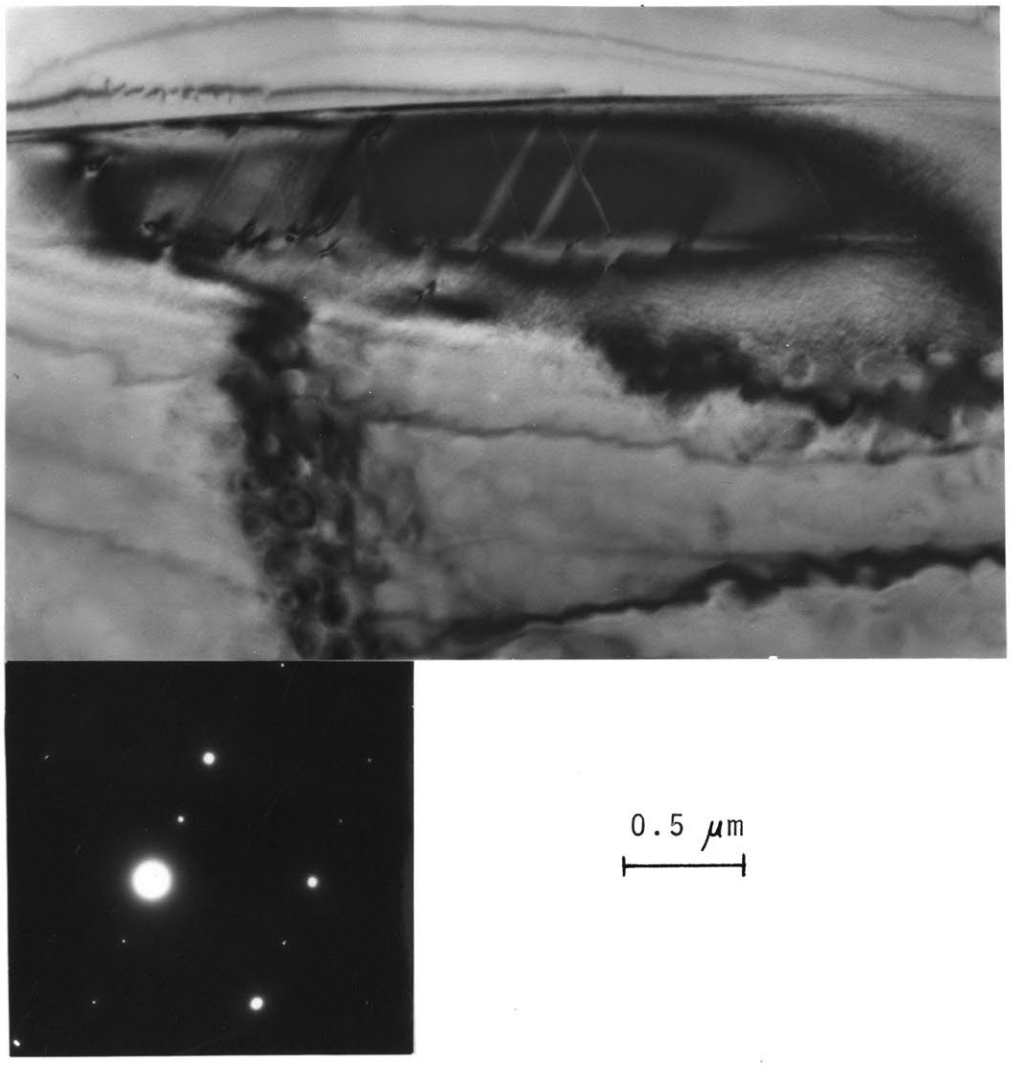

Figure II.4

A bright-field micrograph of the incoherent interface between the Fe_3Al grain boundary layer and the adjacent disordered layer that formed in the specimen shown in Figure II.3. The grain boundary lies along the top edge of the ordered layer in this micrograph. The antiphase boundaries visible in the incoherent ordered layer formed as a result of dislocations moving out of the grain boundary and into the incoherent interface, where many are seen in this micrograph, thus reducing coherency strains.

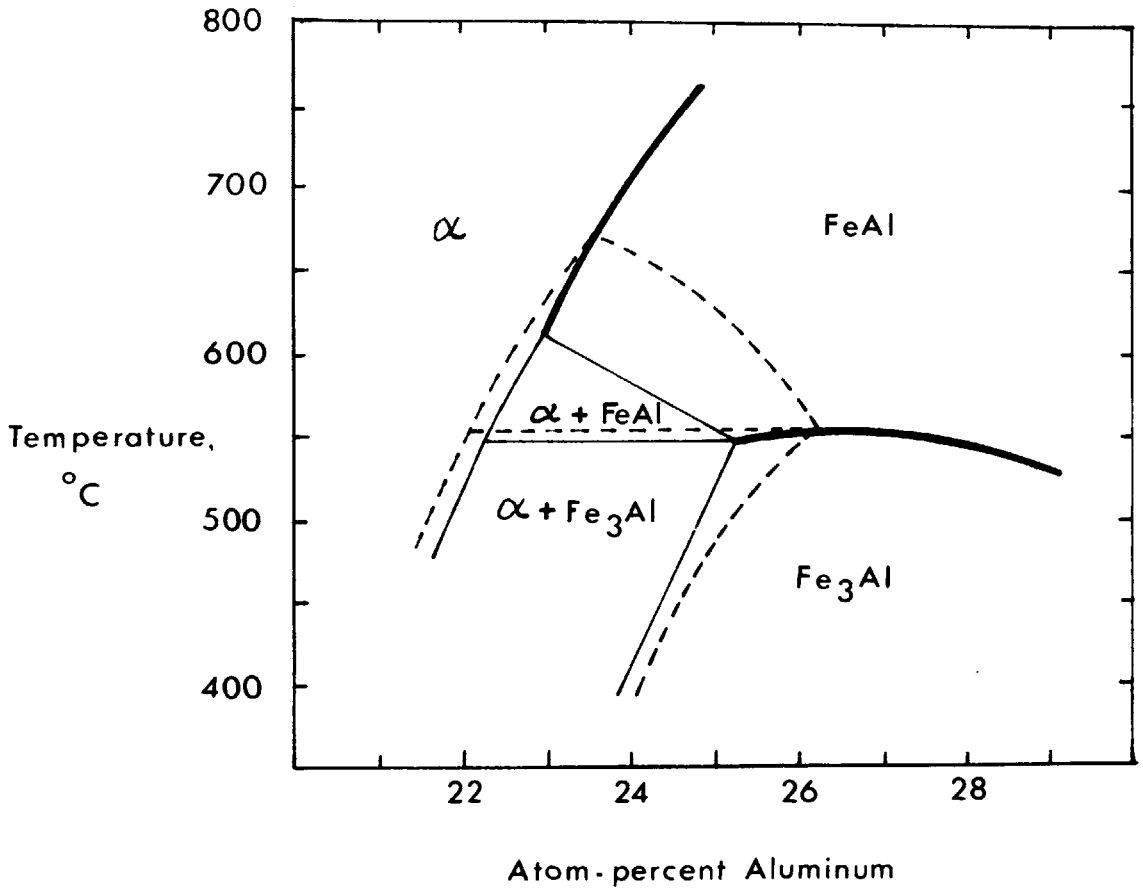

Figure II.5

Proposed form of the composite coherent and incoherent phase diagrams for the iron-aluminum system. The solid lines represent the coherent equilibria, with the heavier lines denoting λ-transitions which are necessarily lines of incoherent equilibria also. The broken lines represent the extent of the incoherent two-phase fields.

III. MECHANISMS OF PHASE TRANSFORMATIONS WITHIN THE MISCIBILITY GAP OF IRON-RICH IRON-ALUMINUM ALLOYS

Abstract

The iron-aluminum system possesses a tricritical point where a line of λ-transitions ends at a miscibility gap at about 23 atom percent aluminum and 615°C. Rules of general applicability governing phase separation within the miscibility gap of such a system are developed. Application of the rules to the iron-aluminum system results in detailed predictions about the mechanisms of decomposition and their sequences in this system. Electron microscopy is used to study the reactions experimentally and the results are in agreement with theoretical predictions.

III.1 Introduction

The order-disorder transitions in the iron-rich iron-aluminum alloys were first reported in 1932 by Bradley and Jay.[1] Since that time, much effort has been put into understanding order-disorder transformations in general and the transitions in iron-aluminum alloys in particular. Because the iron-aluminum system is rather atypical as far as metallurgical order-disorder systems are concerned, the phase diagram for these alloys has only recently become firmly established.[2,3,4]

The phase diagram itself, Figure III.1, displays some remarkable features: it has two ordered phases, FeAl (B2, Pm3m) and Fe_3Al (DO_3,Fm3m), and the transitions α (disordered b.c.c.) → FeAl and FeAl → Fe_3Al are λ-transitions

(higher-order transitions) for appropriate alloys; the line of λ-transitions for the $\alpha \rightarrow$ FeAl transition ends in a symmetrical tricritical point,[5] and below this point the transition between the same phase is first order (in the sense of Ehrenfest[6]).

Electron microscopy studies of these alloys have demonstrated a surprisingly wide variety of microstructures for alloys with compositions from 22 to 25 atom percent aluminum with varying heat treatments and alloy compositions.[7-12] In general, these investigations have been concerned with establishing the phase diagram for these alloys; consequently the principles governing the evolution of microstructures in these alloys have not yet been fully explained. This is the intent of the present work: to show that the currently accepted phase diagram is qualitatively correct, and that an understanding of the thermodynamics from which the phase diagram derives can be applied to predict the transformation mechanisms and consequently the morphologies that will develop from a given heat treatment.

The following format will be adopted in this paper: Section III.2 will comprise a review of the literature which is pertinent to this study; Section III.3 will be an in-depth discussion of the phase diagram and related thermodynamics and kinetic principles which will allow general rules governing decomposition in systems with tricritical

points to be developed; Section III.4 outlines the experimental procedures used in this study; Section III.5 applies the rules developed in Section III.3 to predict the mechanisms of specific transitions in the Fe-Al system and presents the results of electron microscopy observations in support of the predictions; and discussion of the results and the conclusions of this study are stated in Sections III.6 and III.7.

III.2 Literature Review

The most thorough study of the microstructural aspects of the order-disorder transitions in iron-aluminum alloys was the work of Swann, Duff, and Fisher[12] (SDF) who used electron microscopy to accurately characterize the phase diagram for alloys from 22 to 32 atom percent aluminum. As was shown in Chapter II the phase diagram derived from their study is a coherent phase diagram and is the one that is usually observed for short heat treatment times, and applies to this present study. In addition to the unusual phase diagram, the SDF results display a great variety of microstructures suggestive of different mechanisms of phase transformations for these alloys.

Figure III.2, taken from the work of SDF,[11] is a remarkable series of electron micrographs taken from specimens of an Fe-26.5% Al alloy which were equilibrated at the indicated temperatures spanning a range which includes the

critical temperature for the B2 → DO_3 transition. Taken together, the micrographs show all the characteristics of a λ-transition: the gradual disappearance of 1/2 a_o' [100] antiphase boundaries as the critical temperature for DO_3 order is exceeded, no coexistance of the ordered phases, and quenched-in fluctuations of order which increase in intensity as the critical temperature is approached. These results and the results of other experiments by SDF[12] have shown that the transitions α → B2 and B2 → DO_3 are λ-transitions in appropriate alloys. Thus the SDF results demonstrate that two continuous ordering transitions can occur in these alloys.

The SDF results also suggested that spinodal decomposition may occur in some alloys within the miscibility gap (two-phase region of the phase diagram) between the α and FeAl phases. Figure III.3 shows their results for a Fe-23.5% Al alloy, initially heat treated to form single-phase FeAl, then held at 592°C for times of 15 minutes and 2 hours. The disordered phase appears to form with a high degree of connectivity and the contrast difference between the ordered and disordered phase increases with time. Since there is no pronounced alignment of the disordered phase in these micrographs, the observed microstructures are suggestive of spinodal decomposition in a system where the strain energy contribution to the free energy is small.[13] Thus the results of SDF also suggest that a continuous phase separation

mechanism may occur in these alloys.

Figure III.3 also demonstrates that antiphase boundaries are favored sites for the formation of the disordered phase when the FeAl phase decomposes within the α + FeAl region of the phase diagram. The long dark lines in the micrographs are the disordered phase which has formed where 1/4 a_o' [111] antiphase boundaries existed in the single-phase ordered structure. Both SDF[2,12] and Warlimont[9] have reported this phenomenon in the decomposition of FeAl and Fe_3Al.

By and large, X-ray studies of iron-aluminum alloys have dealt primarily with establishing the equilibrium relationships for the observed phases. An exception is the work of Oki, Hasaka, and Eguchi[15] who have studied the time variation of intensities and half-widths of superlattice and fundamental reflections of samples equilibrated at one point in the phase diagram, then quenched and aged for various times in another region of the phase diagram. Their results show that in certain cases the transitions seem to proceed in steps, consistent with the idea of competing mechanisms with different time constants for the transitions from one equilibrium state to another.

Thus, evidence in the literature shows that microstructures in these alloys may be governed by a number of phenomena, and certainly competing reactions may be expected

to play a part. Starting from these experimental observations and considering the form of the phase diagram for these alloys and the results of thermodynamic approximations for the free energy of such systems, we proceed in the next section to make detailed predictions about the mechanisms and microstructures that will result from various heat treatments in these alloys.

III.3 Thermodynamic and Kinetic Principles

In this section we will use the phase diagram and its underlying thermodynamics, along with kinetic principles, to decide which among a limited set of mechanisms will govern the transformations that are possible when a single-phase alloy is made unstable by quenching to a point within the miscibility gap. The set of mechanisms to be considered includes continuous phase changes (ordering and phase separation) and homogeneous and heterogeneous nucleation. In particular a set of rules will be developed which will allow the microstructures observed in particular cases to be understood.

Continuous phase changes can be described by the growth of composition waves. In alloys, two general types of composition waves are observed; those with wavelengths of the order of interatomic spacings, which lead to long-range order, and those with longer wavelengths associated with phase separation. The thermodynamics of a system determines whether or not a system has become unstable with respect to the growth

of such waves.

The first rule which we propose deals with non-equilibrium continuous transitions and is based on the ideas of composition waves of Hillert,[16] Cook, Hilliard, and de Fontaine,[17] and Khachaturyan.[18]

Rule 1: λ-transitions occur continuously regardless of whether the transition is occurring reversibly or not.

The definition of a λ-transition is concerned with the reversible transition. At equilibrium the two phases have become identical and it is meaningless to speak of a mechanism of phase change. If we start with either phase and rapidly change temperature we will achieve nonequilibrium states that can relax towards equilibrium continuously.

Below the order-disorder transition temperature for a λ-transition, there is no nucleation barrier to ordering; likewise for disordering above the transition temperature.

Continuous ordering is a diffusional process involving the growth of amplitude of composition waves with wavelengths on the order of interplanar spacings. Continuous ordering may involve more than one composition wave, in which case the formation of one wave preceeds the other; in some cases for thermodynamic reasons, in other cases for kinetic reasons (see discussion following Rule 2).

The following rule, which we believe to be general, is also adopted.

Rule 2: Where a line of λ-transitions impinges on a miscibility gap, the λ-transition line continues metastably into the two-phase region. When a single phase is brought below such a metastable line within a miscibility gap, the metastable λ-transition will preceed phase separation.

In phase diagrams, metastable extensions of phase boundaries are justified thermodynamically. Because the diffusion distance involved in continuous ordering is very small, metastable continuous ordering transitions occur more rapidly than phase separation, provided that the metastable ordering lines have been crossed by a small but finite amount.

In iron-aluminum alloys, two of the metastable continuous ordering curves are easy to locate, these being the extension of the equilibrium lines of λ-transitions into the two-phase regions of the phase diagram.

In systems like Fe-Al, where more than one continuous transformation is possible, we introduce the concept of conditional and unconditional continuous reaction curves. For the purpose of the definitions, the initial state of the alloys is always taken to be the homogeneous disordered phase α. The critical curve for DO_3 ordering in the Fe-Al phase diagram is a conditional curve because its location is dependent on the condition that $\alpha \rightarrow$ B2 ordering has occurred. We denote the critical curve for formation of an ordered phase from the disordered single phase an unconditional ordering curve. Thermodynamically an unconditional ordering curve must exist for the direct conversion of α to DO_3 but

its location has not been determined experimentally or theoretically for the Fe-Al system.

The theory of continuous phase separation in systems with ordinary critical points is well established;[19] coherent spinodals have been calculated and measured in such systems.[20] In systems with tricritical points like Fe-Al the theory is not well established. With the exception of the work of Richards[21] and Richards and Cahn,[22] the statistical thermodynamics of ordering systems has mainly been concerned with establishing phase diagrams, and not lines of instability. Thus it is instructive to relate Richards' results to the iron-aluminun system.

The model investigated by Richards assumes pairwise interactions between first and second neighbor atoms. In particular the interchange energies V_1 and V_2 were chosen so that V_1 favored formation of unlike pairs and V_2 favored the formation of like pairs of atoms. The ground state in this case is two-phase, α + B2.[21,23,24] The free energy, f, in Bragg-Williams' approximation[21,22] was investigated as a function of composition, c, and long range order parameter, s, for different temperatures. A projection onto the f-c plane of the locus of minima in the resulting free energy surface at a temperature T* within the miscibility gap near the tricritical point is shown schematically in Figure III.4. Within the disordered phase $\left.\frac{\partial^2 f}{\partial c^2}\right|_{s = 0}$ is always positive and the

alloy is stable with respect to continuous phase separation. At the continuous ordering transition f and $\frac{df}{dc}$ are continuous but $\frac{d^2f}{dc^2}$ is discontinuously lower for the ordered phase. At the tricritical point $\frac{d^2f}{dc^2}$ is zero for the ordered phase. Below the tricritical point, at the composition where metastable continous ordering becomes possible, $\frac{d^2f}{dc^2}$ is positive in the disordered phase and changes sign in the ordered phase. Therefore, once the alloy is ordered, it is unstable with respect to spinodal decomposition, and this model indicates that one branch of the spinodal curve is the metastable extension of the continuous ordering curve for the $\alpha \rightarrow$ B2 transition. Thus, in this model the phase diagram contains conditional spinodals; conditional in the sense that the alloy must first be ordered before spinodal decomposition is possible. We believe that this type of behavior is model-independent, and will occur in any ordering system where a line of λ-transition ends at a miscibility gap. Such tricritical points have been shown to exist in phase diagrams calculated assuming that both interchange energies favor formation of unlike pairs of atoms[25,26], as in iron-aluminum alloys.[27] Therefore, we make the following rule.

Rule 3: In a system having a tricritical point where a line of λ-transitions for ordering ends in a miscibility gap, there is a conditional spinodal. One of the spinodal curves is the metastable extension of the line of λ-transitions, and the other spinodal curve may be approximated by theoretical methods. Spinodal decomposition can occur only on the condition that ordering has occurred.

The next rules are of general validity for all miscibility gap systems.

Rule 4: Within a miscibility gap phase separation must occur by nucleation and growth of the second phase unless the spinodal condition has been met.

Rule 5: The morphologies that develop within the spinodal may be radically affected by inhomogeneities on a scale comparable to the spinodal wavelength.

Within the spinodal the diffusion equation for spinodal decomposition[28] will apply. Since the spinodal is conditional on the existence of the ordered phase, the initial state to which the diffusion equation is applicable within the spinodal will certainly not be valid if the initial distribution of heterogeneities is of the same order, or smaller than, the spinodal wavelength.

In the iron-aluminum system Rule 5 is particularly important because of the known tendency for iron to segregate to antiphase boundaries[9,2]. We shall show that the disordered phase often wets these boundaries and that they are therefore sites for easy nucleation of the disordered phase. Since metastable continuous ordering results in an APB size that is of the same order as the spinodal wavelength, in specimens which have undergone metastable continuous ordering within the spinodal segregation on APBs may prevent the attainment of the periodic morphologies associated with spinodal decomposition.

It is our hypothesis that the preceding rules are of general validity for ordering systems possessing tricritical

points where a line of λ-transitions ends in a miscibility gap. Recognition of this fact is required if the mechanisms of the transitions and resulting morphologies in systems like iron-aluminum are to be understood.

On the basis of the given rules it is possible to draw the phase diagram shown in Figure III.5. The metastable continuous ordering lines (labelled 1) and the right-hand spinodal line (labelled 2) are drawn schematically. The right-hand spinodal curve ends at its intersection with the metastable continuous ordering line for the FeAl $\rightarrow$ Fe_3Al transition on the basis of Rule 2. The additional lines in the phase diagram partition the diagram into ten separate areas, labelled a-j in Figure III.5, which are convenient for classification of the possible decomposition reactions in various alloys in conjunction with the five rules.

The reactions to be discussed all involve a single-phase initial state, on the basis that the number of such transitions is limited and easy to classify. In addition, for sufficiently coarse two- or multi-phase initial states, each phase will transform independently and within each phase the reactions would proceed according to the five rules. For very fine two-phase initial states, or states that cannot be classified as consisting of homogeneous equilibrium phases, the transitions could be highly morphology dependent, and classification of reactions would be difficult.

Table III.1 is a summary of the decomposition mechanisms expected to occur starting from a single-phase state. The first column lists the phases present in the initial and final states. The second column lists the particular initial and final states relative to the metastable continuous ordering lines and spinodal curves by referring to the lettered areas a-j shown in Figure III.5. The mechanism for each phase change is listed in the third column, derived from the applicable rules which are indicated in the final column.

The following sections will discuss in detail the application of the rules to each of the transitions listed in Table III.1. In addition, experimental evidence of the rules' usefulness for predicting the transformed morphologies will be presented for those cases that have been investigated in the present work or by earlier studies. First, the experimental procedures of the present study will be discussed.

III.4 Experimental Procedures

Alloys of 23.0 and 24.0 atom percent aluminum were prepared at the General Electric Research and Development Center from 99.99% Fe and 99.999% Al by vacuum induction melting. Ingots were chill cast into 2.5 cm diameter molds, then hot swaged to 5 mm diameter rods. The as-received microstructure was approximately 50% recrystallized. Pieces of the rod were machined to 3 mm diameter, then given a

15 minute disordering treatment in argon at 725°C and rapidly quenched into water.

Except where indicated otherwise, single-step heat treatments, and the first step of two-step heat treatments were carried out as follows:

Discs 0.25 mm thick were cut from the rod by EDM, then polished by hand to remove the spark-affected zone. The discs were then sealed in evacuated capsules. The encapsulated specimens were heat treated in a vertical furnace that was equipped for rapid quenching. Quenching was accomplished by ejecting the capsule out the bottom of the furnace into a cold brine quenchant. Submerged in the brine was a heavy metal object placed so that the capsule was broken immediately upon entering the quenchant.

The second step of the two-step heat treatments was performed by sealing the quenched discs in 50 μm stainless steel foil and heat treating in molten lead. Quenching was accomplished by rapidly transferring the wrapped specimens out of the lead pot into cold brine.

Electron microscopy specimens were prepared using a double jet electropolisher with an electrolyte of two parts methanol to one part nitric acid. Polishing temperature was -40 to -50°C and current densities were in the range of 0.5 - 1.5 amp/cm^2.

Electron microscopy was done at 100 KV using a JEM 7.

Since each specimen used in this study was given an initial disordering anneal, then rapidly quenched prior to aging, the as-quenched state prior to aging is of interest. Figure III.6 is a (200) dark-field micrograph and selected-area diffraction pattern of an Fe-23% Al alloy rapidly quenched from 725°C. The micrograph shows that FeAl ordering during the quench is not completely suppressed, and that the ordered phase consists of a fine dispersion of ordered regions having a maximum size of about 200Å in a disordered matrix. The selected-area diffraction pattern shows sharp superlattice reflections from the FeAl phase.

Comments are in order concerning the contrast conditions required for revealing the ordered phases and the antiphase boundary (APB) structures in the B2 and DO_3 superlattices. Marcinkowski and Brown[29] made the first detailed electron microscopy study of the antiphase boundary structures in the FeAl and Fe_3Al phases. The length a_o' of the unit cell of Fe_3Al (F m3m, 16 atoms per unit cell) is twice that of FeAl and of α. We will index all reflections to this large superlattice. The fundamental α (I m3m) reflections occur for $h + k + l = 4n$. The FeAl (P m3m) superlattice reflections occur for $h + k + l = 4n + 2$. The Fe_3Al reflections occur for h, k, and l unmixed. When h, k, l are even the reflection coincides with either fundamentals or FeAl reflections. When h, k, l are all odd the reflection

belongs to Fe_3Al alone. In the Fe_3Al phase two types of APBs occur, having $\frac{a'_o}{4}$ [111] and $\frac{a'_o}{2}$ [100] displacements. Both types may be observed in dark-field electron microscopy by imaging a superlattice reflection for which h, k, and l are all odd. Only the $\frac{a'_o}{4}$ [111] APBs are observed when a superlattice reflection is imaged for which $(h+K+l)= 4n + 2$. The FeAl phase has only the $\frac{a'_o}{4}$ [111]- type APBs which are observed in dark-field images formed from a superlattice reflection for which $(h+k+l) = 4n + 2$.

III.5 Application of the Proposed Rules to the Iron-Aluminum System

The purpose of this section is to show how the rules developed in the previous section can be applied to specific decomposition reactions in iron-aluminum alloys, and to show that the predicted transformation mechanisms are consistent with the observed morphologies.

It will be convenient to discuss the transitions possible from single-phase B2 initial states first, taking into account differences in transformation behavior which are dependent on initial antiphase domain size (Rule 5).

The transitions listed in Table III.1 will now be considered in turn.

$$B2 \rightarrow DO_3$$

The transition b → j, Figure III.5, has been shown by SDF[11] and Guttman et. al.[30] to be a λ-transition. Therefore by Rule 1, it must proceed by continuous ordering. Specifically, it will continuously order by the growth of composition waves of wavelength a'_0 (1/2 1/2 1/2), where a'_0 is the lattice parameter of the 16 atom unit cell of the DO_3 phase. The metallography of the transition has been studied in detail by SDF,[11] and some of these results are shown in Figure III.2.

$$B2 \rightarrow \alpha + B2$$

In the transition b → d, Figure III.5, single-phase B2 is decomposed within the conditional spinodal. Since the condition for spinodal decomposition is met (Rule 3), the resulting morphology will be governed by the initial B2 antiphase domain size (Rule 5). For coarse initial domain sizes, the two-phase morphology will develop according to the theory of spinodal decomposition[19] and have a characteristic wavelength and (possibly) alignment.

The following experiment was performed to test these predictions. Strips of Fe-24% Al sheet were aged for one hour at 625°C in molten lead to produce a single-phase FeAl microstructure. Specimens were then quenched directly into another lead pot at 570°C and aged for times of 10 seconds,

1 minute, and 5 minutes prior to quenching in cold brine. Figure III.7 shows dark-field micrographs imaging superlattice reflections from the FeAl phase for the three aging treatments; thus the FeAl phase appears light and the α phase appears dark. The microstructures appear to be the result of a continuous decomposition process, and the morphology is like that of spinodal decomposition in a system where the elastic energy contribution to the free energy is small.[13]

No diffuse intensity is observed in the selected area diffraction patterns which can be correlated to a characteristic wavelength of the microstructure (i.e. sidebands). This is not suprising if the morphology is truly isotropic, for the diffuse intensity would be in the form of spherical shells around fundamental reflections and thus hard to observe. The diffracting conditions for the micrographs in (b) and (c) are nearly identical; in both cases the specimen was oriented close to the [100] pole. This orientation could not be obtained in (a), which was taken near the [110] pole.

The three aging times were used in an attempt to prove by the microstructural sequence method[31] that spinodal decomposition had occurred; however, if indeed the mechanism is spinodal as we expect, the time interval over which the decomposition occurs at constant wavelengths was not observed in these experiments. We thus conclude that the experimentally observed decomposition process appears to be continuous but

that its exact nature is not yet established.

For initial B2 domain sizes on the order of the spinodal wavelength the morphology of the b → d transition will be strongly affected by segregation of iron to the APBs (Rule 5). In particular, this effect will be enhanced within the spinodal and the morphology should consist of the cores of the two initial domains separated by a layer of the disordered phase.

The transition b → e, Figure III.5, occurs outside the spinodal and therefore must occur by nucleation and growth of the disordered phase (Rule 4). For specimens with large initial B2 domain sizes the disordered phase is expected to form both homogeneously within the domains and heterogeneously at the APBs. The morphology will consist of coherent regions of α within single domains of the B2 phase, along with a layer of α coating the APBs. Specimens with small initial domain sizes are expected to decompose chiefly by the precipitation of α on APBs, thus leaving the two initial domains separated by a layer of α.

$$B2 \rightarrow \alpha + DO_3$$

In the transition b → g, Figure III.5, single-phase B2 is decomposed within the conditional spinodal. Since the condition for spinodal decomposition is met (Rule 3), the

resulting morphology will be governed by the initial anti-phase domain size (Rule 5). For coarse initial domain sizes, the transition will proceed as follows. Spinodal decomposition will occur first. Then as the composition of the aluminum-enriched regions increases, these regions will undergo continuous DO_3 ordering (Rule 2). The microstructure that is developed in a Fe-24% Al alloy that is initially single-phase B2, then aged at 539°C for 150 seconds, is shown in Figure III.8. Figure III.8(a) shows a (222) dark-field micrograph showing that continuous decomposition of the initial B2 domains has occurred resulting in a spinodal-like microstructure where the ordered material is bright and the disordered is dark. Figure III.8(b) shows a (111) dark-field micrograph of the same structure, revealing the small domains of the DO_3 phase that have formed in the aluminum-enriched regions. Thus, there is good agreement between the proposed mechanism and the observed morphology for this reaction.

For initial B2 domain sizes on the order of the spinodal wavelength, Rule 5 dictates that the spinodal morphology will be altered. In particular, segregation of iron to the original $\frac{a'_o}{4}$ [111] APBs, forming α, will occur initially. As the composition of the initial domain cores increases, these will undergo metastable continuous ordering to DO_3 (Rule 2) followed by continued precipitation of α on APBs, including the newly formed $\frac{a'_o}{2}$ [100] APBs. The

morphology will thus consist of the domain cores separated by layers of the α phase. Depending on the proximity of the overall alloy composition to the metastable DO_3 continuous ordering line, there may be a detectable difference in thickness of the α layers formed on the $\frac{a'_o}{4}$ [111] and the $\frac{a'_o}{2}$ [100] APBs. The former should be thicker, the further the alloy composition is from the DO_3 ordering curve (i.e., the higher the temperature).

The transition b → h, Figure III.5, occurs outside the spinodal and thus must proceed by nucleation and growth (Rule 4) of the disordered phase. For large initial B2 domains, homogeneous nucleation and growth of coherent α within the domains and heterogeneous precipitation of α will occur at the necessary undercooling. As the aluminum content of the remaining B2 increases it will undergo metastable continuous ordering to DO_3, followed by additional precipitation of α on the newly formed $\frac{a'_o}{2}$ [100] APBs. The morphology will consist of large $\frac{a'_o}{4}$ [111] domains containing coherent α regions and smaller $\frac{a'_o}{2}$ [100] domains. All APBs will be coated with a layer of the disordered phase, and specimens transformed at higher temperatures should have less α on the $\frac{a'_o}{2}$ [100] APBs than on the $\frac{a'_o}{4}$ [111] APBs. Specimens with initial B2 domain sizes that are small will precipitate the α phase heterogeneously on APBs, then the aluminum-enriched B2 will continuously order to DO_3, followed by continued precipitation

of α on the $\frac{a'_o}{2}$ [100] APBs. Except for the absence of the homogeneously nucleated α and the change of scale, the resulting morphology should be analogous to that produced in the same transition with large initial B2 domains.

The transition b → i, Figure III.5, begins by metastable continuous ordering to DO_3 (Rule 2). Because of the fine domain size that this produces and the tendency for segregation of iron to APBs, phase separation will occur by the heterogeneous precipitation of the disordered phase on APBs. The morphology of transformed specimens with initially coarse B2 domains and initially fine B2 domains will be basically the same: a fine APB structure will show the domain cores separated by a layer of the α phase. Figure III.9 shows the microstructure of a Fe-24% Al alloy, initially heat treated to produce single-phase B2, that was aged at 475°C for 300 seconds. Figure III.9(a) shows a (111) dark-field micrograph which reveals the Fe_3Al ordered domains. Figure III.9(b) is a (222) dark-field micrograph of the same specimen. The broad dark APB was present in the initial FeAl structure, and the contrast within the original domains is due solely to the presence of a layer of the disordered phase formed as a result of the b → i transition. The $\frac{a'_o}{2}$ [100] APBs thus delineated would normally show no contrast when viewed with a (222) reflection.[29] Thus the experimentally observed microstructure is consistent with

the proposed mechanism.

$\alpha \rightarrow B2$

The equilibrium $\alpha \rightarrow B2$ transition has been shown to possess the microstructural characteristics of a λ-transition by Swann, Duff, and Fisher.[12]

Unfortunately FeAl order is very difficult to suppress during a quench and thus this transition is not a good one to choose for studying the non-equilibrium continuous reaction. By Rule 1, the non-equilibrium $\alpha \rightarrow B2$ ($d \rightarrow b$ in Figure III.5) transition should occur by continuous ordering, specifically by the growth of a_o [100] composition waves, where a_o is the lattice parameter of the b.c.c. lattice. Although the specimen shown in Figure III.6 is not one that received a well defined isothermal heat treatment, by Rule 1 it should be a good representation of partial order by a continuous ordering mechanism. We believe that the particulate nature of the microstructure reflects the ordering brought about by individual vacancies consistent with the findings of Beeler[32] and is not the result of a metastability of the disordered phase with respect to continuous change of order.

$\alpha \rightarrow \alpha + B2$

The $\alpha \rightarrow \alpha + B2$ transition, a → c in Figure III.5, involves decomposition within the miscibility gap, but outside the spinodal. Hence by Rule 4 the ordered phase must form by nucleation and growth. Since well annealed disordered samples have few heterogeneous nucleation sites the nucleation should be random; considering the low volume fraction of the ordered phase in region c the two-phase morphology should be a dispersion of ordered particles in a disordered matrix. This is the morphology that is observed experimentally. Figure III.10 shows a (200) dark-field electron micrograph from the SDF study[12] for this transition.

Since the transitions a → d and a → e must first involve metastable continuous ordering (Rule 2), subsequent phase separation will proceed as if the specimen were initially single-phase B2 with very small initial domain size. The expected morphology was thus discussed previously under the b → d and b → e transitions. The microstructure developed in an initially disordered Fe-23% Al alloy after aging for 160 minutes at 570°C is shown in Figure III.11. The high connectivity within the ordered phase results from the fact that only two domains are present in the FeAl phase, and each connected region is part of one domain, explaining the absence of antiphase boundaries in this structure. It is worthwhile to note that the microstructure in Figure III.11 might be assumed to be associated with spinodal decomposition

in a system where the elastic energy was not significant;[13] the absence of APBs in the ordered phase belies a spinodal mechanism.

$$\alpha \rightarrow \alpha + DO_3$$

We first consider the transition a → f, Figure III.5. Analogous to the $\alpha \rightarrow \alpha$ + B2 transition a → c discussed above, we expect this transition to occur by homogeneous nucleation and growth, according to Rule 3. As anticipated, experimental observations[9] of microstructures developed after these transitions show dispersions of DO_3 particles in a disordered matrix. No observations of B2 nuclei have been reported to date.

It is likely that the critical nucleus for this transition would be ordered DO_3. However, depending on the explicit form of the volume and interfacial free energies, it is possible that the critical nucleus could be ordered B2, in which case the growing ordered particle would at some point become unstable with respect to continuous ordering to DO_3.

The transitions a → g and a → h, Figure III.5, will begin by metastable continuous ordering, resulting in a small domain size B2 ordered structure. The phase separation reactions from this state have been discussed under the transitions b → g and b → h. The two-phase morphology

observed in an initially disordered and quenched Fe-23% Al sample aged for 150 minutes at 530°C is shown in Figure III.12. As expected, this (111) dark-field micrograph shows a highly interconnected two-phase morphology, $\alpha + DO_3$. The selected area diffraction pattern ([110] normal to foil) shows that the FeAl superlattice reflections are much more intense than those from the Fe_3Al phase. This can be attributed to the fact that at 530°C the composition of DO_3 in equilibrium with α is close to the B2 $\rightarrow$ DO_3 λ-line and therefore the superlattice spots should reflect the low long-range DO_3 order. In line with this explanation, the micrograph also shows faint contrast within the ordered phase suggestive of APBs, presumably the 1/2 a'_o [100] - type; although overlap of adjacent ordered domain through the thickness of the thin foil could cause the same effect.

In the transition a $\rightarrow$ i, Figure III.5, metastable B2 continuous ordering will also occur first, resulting in a fine-domain B2 structure which will phase separate according to the mechanism discussed under the b $\rightarrow$ i transition. No observations of the early stages of this transition are available; however, Figure III.13, taken from the work of SDF[12], shows the microstructure developed in a Fe-24.1%-Al alloy held at 452°C for 64 hours, demonstrating that a thin layer of α has formed in all APBs, as expected.

$\alpha \rightarrow DO_3$

In the $\alpha \rightarrow DO_3$ transition, a → j in Figure III.5, two lines of λ-transitions are crossed and therefore by Rule 1 the transition occurs by successive continuous ordering reactions. First an a_o <100> composition wave is established, creating B2 long range order, then an a'_o <1/2 1/2 1/2> wave develops, creating DO_3 long range order. The morphology developed has large $1/4a'_o$ [111] antiphase domains enclosing many $1/2a'_o$ [100] antiphase domains, as shown in Figure III.14 (from the work of Swann, Duff, and Fisher[12]).

It is worthwhile to note that there may exist thermodynamic states in which the DO_3 phase forms continuously from α by unconditional a'_o <100> continuous ordering, followed by the growth of the a_o <100> composition wave. In this way a B32 (NaTl) instead of B2 superlattice would be established prior to the DO_3. In this case, $1/4a'_o$ [111] domains would be observed within larger $1/2a'_o$ [100] domains, the reverse of that which is observed.

III.6 Discussion

This study represents a first attempt at a detailed investigation of the mechanisms of phase transitions within the miscibility gap of a system possessing a symmetrical tricritical point. Applied to iron-rich iron-aluminum

alloys the theoretical predictions are born out experimentally. It is worthwhile to point out some very basic results of this study.

One possibly surprising result is that a disordered alloy held within the miscibility gap may first transform to a completely ordered state before the phase separation occurs. This is a consequence of the metastable continuous ordering reactions that occur in this system, and the absence of classical nucleation of the ordered phase from the disordered.

The present results also clearly demonstrate that ordering and clustering (i.e., spinodal decomposition) are not opposites but can occur in the same system and even concurrently (Figure III.8). We have shown that an understanding of the thermodynamics of this system has allowed the sequences of decomposition and ordering reactions to be selected for some alloys. Thus the transition $B2 \rightarrow \alpha + DO_3$ has been made to occur by continuous decomposition first, followed by ordering, and vice-versa. The key to understanding the transformation sequences in this system is recognizing that both metastable continuous ordering lines and a conditional spinodal are implied by the phase diagram.

There are other systems which have been reported to undergo both ordering and clustering reactions, such as Cu-Be,[33] Ni-Mo,[34] and Cu-Ti.[31,35] A "tweed" morphology, thought to be indicative of ordering occurring first in systems

where the ordered phase is non-cubic, develops in some of these systems,[33,34] while in others[31,35] spinodal decomposition preceeds ordering. Based on our results for iron-aluminum alloys, it may be possible to alter the sequence of ordering and decomposition in these other systems by using different heat treatments or alloy compositions.

The metallographic aspects of continuous ordering transformations are still somewhat of an unknown with regard to an atomistic model. Presumably diffusion via a vacancy mechanism is required for the growth of short-wavelength composition waves. We believe that this is manifested in the microstructure shown in Figure III.6. That specimen was quenched from the disordering temperature of 725°C and a high density of discrete FeAl domains formed during the quench. If ordering during the quench was continuous ordering, as we believe it should have been, why did such a discontinuous microstructure develop? We believe that an answer is provided by a computer model studied by Beeler.[32] In this model a vacancy was introduced into a partially ordered crystal, and it was found that the vacancy was strongly bound to the interface between ordered and disordered material; a single ordered region could grow by the migration of a vacancy around its periphery. Thus in Figure III.6 what we might be seeing is a one-to-one correspondence (approximately) between the density of FeAl particles and the equilibrium

number of vacancies in the alloy at 725°C.

The behavior of the two-phase interconnected morphologies is interesting. On coarsening, the microstructures shown in Figures III.11 and III.12 behave differently. Aging at 570°C involves B2 ordering; there are only two ordered domains present. In a single-phase B2 microstructure the two domains are interlocked and continuous through the whole microstructure. When a second phase forms on the APBs, the domain cores that are left take on the topology of the original domains. In aging at 530°C the DO_3 ordered structure develops and this has four domains which from a strictly topological viewpoint can take on the continuous interconnected morphology of the B2. Thus when phase separation occurs by segregation of iron to APBs the domain core structure left is more discrete in the DO_3 case than the B2; and in coarsening, the $\alpha + DO_3$ structure more quickly loses its highly-connected appearance than the α + B2 structure does. For heat treatments producing comparable diffusion distances, the $\alpha + DO_3$ structure appears more discrete and globular than the α + B2.

The tendency for iron to segregate to APBs can be understood theoretically.[36] It is not clear, however, what name to apply to this method of phase separation in iron-aluminum alloys. It appears that the $1/4a'_o$ [111] APBs are always completely wet by the disordered phase when

it is present hence the term barrierless nucleation would seem to apply. When this method of phase separation occurs within the spinodal, however, it is reasonable to expect that the tendency of iron to segregate to APBs is simply enhanced by uphill diffusion, making the term nucleation misleading. Experimental elucidation of this point no doubt would be difficult.

Complete wetting of the $1/2a'_o$ [100] APBs also appears to occur at early aging times for some heat treatments, as seen in Figure III.9. However an initially disordered Fe-23% Al specimen aged at 530°C for 1100 minutes showed definite contact angles at points where $1/2a'_o$ [100] APBs ended at a coherent interphase interface. We believe that when the $1/2a'_o$ [100] APBs are not wetted it is because the ordered DO_3 formed at a point in the phase diagram which was close to the B2 → DO_3 λ-transition line, and therefore the energy of these APBs would be very low.[37] This point will require further investigation.

A final point to be mentioned is the apparent disparity between the existence of two phase diagrams for these alloys,[4] coherent and incoherent, which implies that lattice parameter differences between coexisting phases are significant; and the apparent isotropic morphology of what appears to be spinodal decomposition. Since the temperature-depression of the coherent diagram is known, this should be able to be

related to the strain energies in the types of microstructures that have been observed in these alloys. Since the lattice parameters are known to vary rapidly in the ordered FeAl phase close to the λ-transition,[3] such calculations should be based on an accurate knowledge of the time variations of lattice parameters, order parameters, and compositions of the phases involved at different temperatures. These data are unfortunately not yet available.

III.7 Conclusions

1. A qualitative understanding of the phase transformations in an ordering system with a tricritical point where a line of λ-transitions ends in a miscibility gap must take account of the following:

a. Metastable continuous ordering lines which are extensions of the equilibrium lines of λ-transitions into the miscibility gap exist and are important.

b. Within the miscibility gap, metastable continuous ordering will take precedence over phase separation when thermodynamically possible.

c. Within the miscibility gap, there is a conditional spinodal, conditional in the sense that a thermodynamic requirement for spinodal decomposition is that the alloy be ordered.

d. Within the spinodal the morphology that develops

in an initially ordered alloy may be grossly altered if the initial state contains heterogeneities (i.e., antiphase boundaries) on a scale that is comparable to the spinodal wavelength.

2. The above general principles can be applied successfully to transitions in iron-aluminum alloys having 22-25 atom percent aluminum and used to predict morphologies resulting from specific heat treatments.

III.8 References

1. A.J. Bradley and A.H. Jay, Proc. Roy. Soc. London A 136 210(1932).

2. P.R. Swann, W.R. Duff, and R.M. Fisher, Trans. TMS-AIME, 245, 851(1969).

3. H. Okamoto and P.A. Beck, Met. Trans. 2, 569(1971).

4. Present work, Chapter II.

5. R.B. Griffiths, J. Chem. Phys. 60, 195(1974).

6. P. Ehrenfest, Communications Leiden, Suppl. 756(1933). See discussion in: Epstein, Thermodynamics, p.128-133, (New York, Wiley, 1937).

7. G. Lutjering and H. Warlimont, Z. Metallk. 56, 1(1965).

8. P.R. Swann and R.M. Fisher, Appl. Phys. Lett. 9, 279 (1966).

9. H. Warlimont, Z. Metallk. 60, 195(1969).

10. H. Warlimont, H. Muhe, and H. Gengnagel, Z. Ang. Physik 26, 301(1969).

11. P.R. Swann, W.R. Duff, and R.M. Fisher, Phys. Stat. Sol. 37, 577(1970).

12. P.R. Swann, W.R. Duff, and R.M. Fisher, Met. Trans. 3, 409(1972).

13. J.W. Cahn, J. Chem. Phys. 42, 93(1965).

14. P. Morgand, Met. Trans. 1, 2331(1970).

15. K. Oki, M. Hasaka, and T. Eguchi, Jap. J. Appl. Phys. 12, 1522(1973).

16. M. Hillert, Acta Met. 9, 525(1961).

17. H.E. Cook, D. deFontaine, and J.E. Hilliard, Acta Met. 17, 765(1969).

18. A.G. Khachaturyan, Phys. Stat. Sol. (b) 60, 9(1973).

19. J. Hilliard, Phase Transformations, Chapter 12, ASM(1970).

20. K.B. Rundman and J.E. Hilliard, Acta Met. 15, 1025(1967).

21. M.J. Richards, Sc. D. Thesis, M.I.T.(1971).

22. M.J. Richards and J.W. Cahn, unpublished research.

23. M.J. Richards and J.W. Cahn, Acta Met. 19, 1263(1971).

24. S.M. Allen and J.W. Cahn, Acta Met. 20, 423(1972).

25. G. Inden, Acta Met., to be published.

26. R. Kikuchi and C.M. vanBaal, Scripta Met. 8, 425(1974).

27. M.M. Naumova, S.V. Semenovskaya, Sov. Phys. S.S. 13, 312(1971).

28. J.W. Cahn, Acta Met. 9, 795(1961).

29. M.J. Marcinkowski and N. Brown, J. Appl. Phys. 33, 537 (1962).

30. L. Guttman, H.C. Schnyders, and G.J. Arai, Phys. Rev. Lett. 22, 517(1969).

31. D.E. Laughlin and J.W. Cahn, Acta Met., to be published.

32. J.R. Beeler, Phys. Rev. 138, A1259(1965).

33. L.E. Tanner, Phil. Mag 14, 111(1966).

34. P.R. Okamoto, Ph. D. Thesis, Univ. of Calif. Berkeley (1970).

35. D.E. Laughlin, Ph. D. Thesis, M.I.T.(1973).

36. J.W. Cahn and R. Kikuchi, J. Phys. Chem. Solids 20, 94(1961).

37. L. Onsager, Phys. Rev. 65, 117(1944).

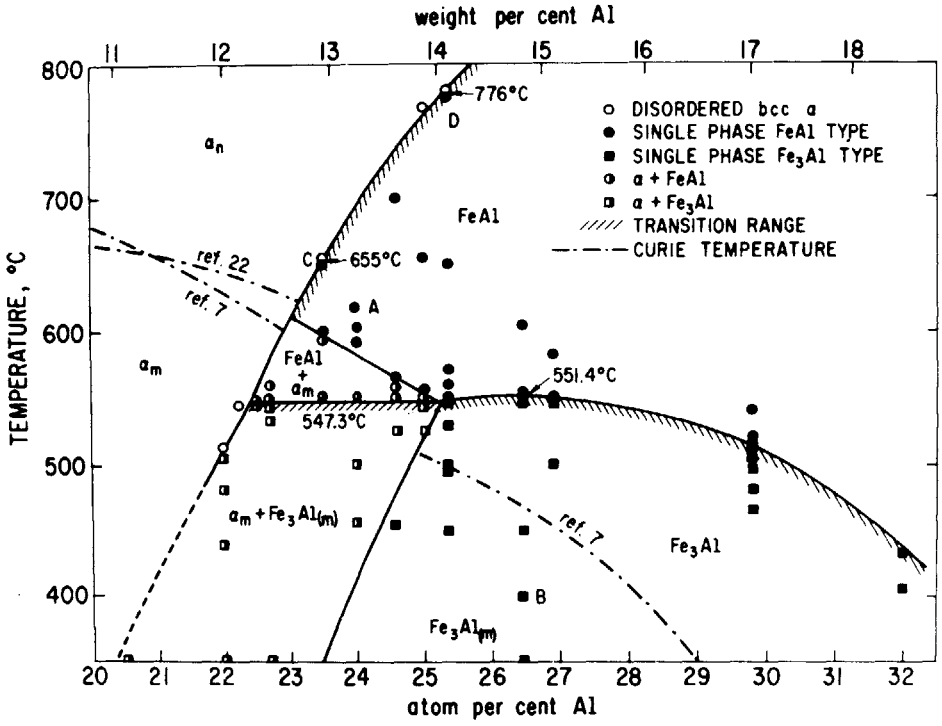

Figure III.1

The iron-aluminum phase diagram based on the electron microscopy study of Swann, Duff, and Fisher (References 2 and 12).

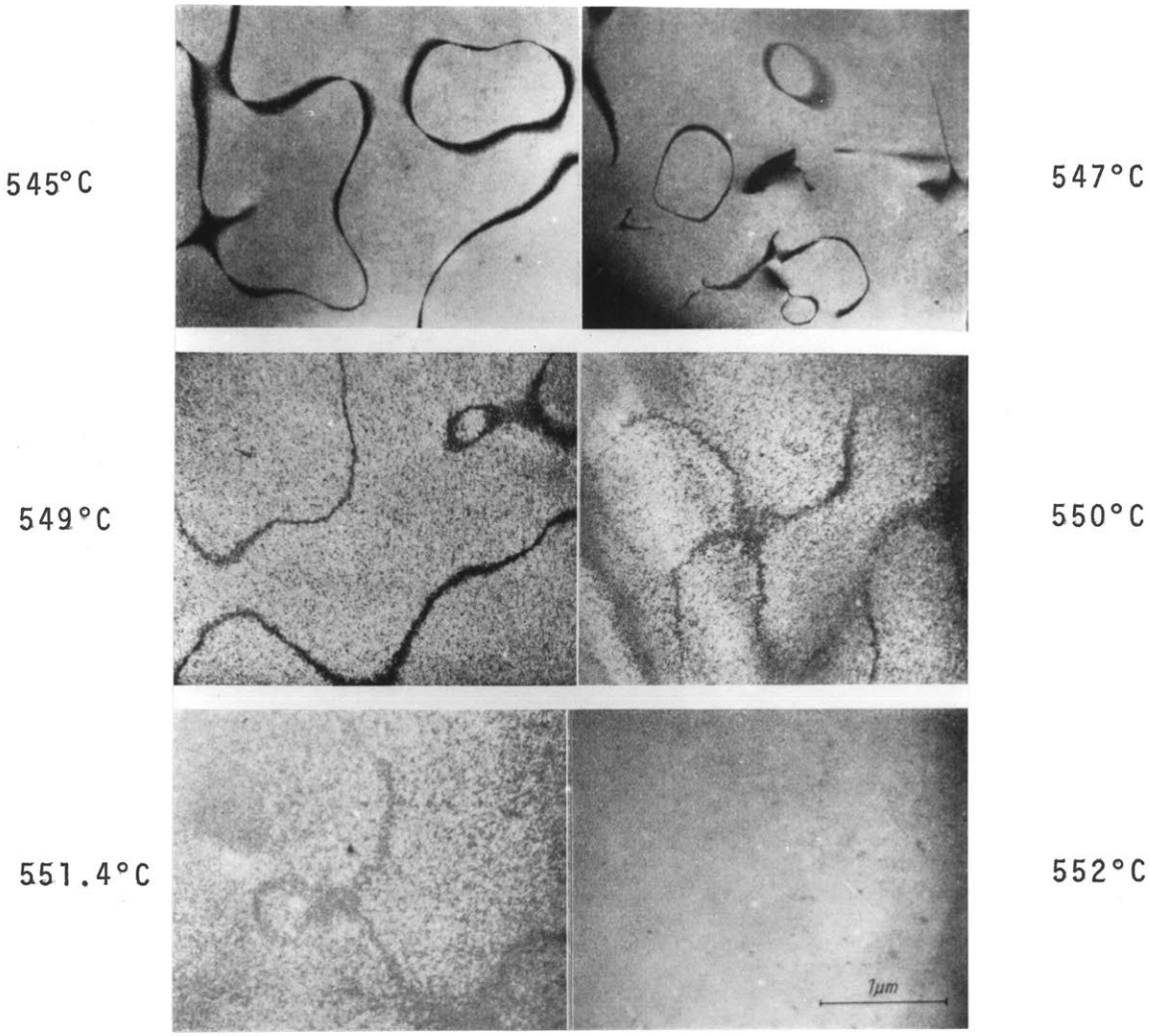

Figure III.2

A sequence of (111) dark-field micrographs from the Swann, Duff, and Fisher study showing microstructures of an Fe-26.5% Al alloy, equilibrated at the indicated temperatures and quenched.

(a)

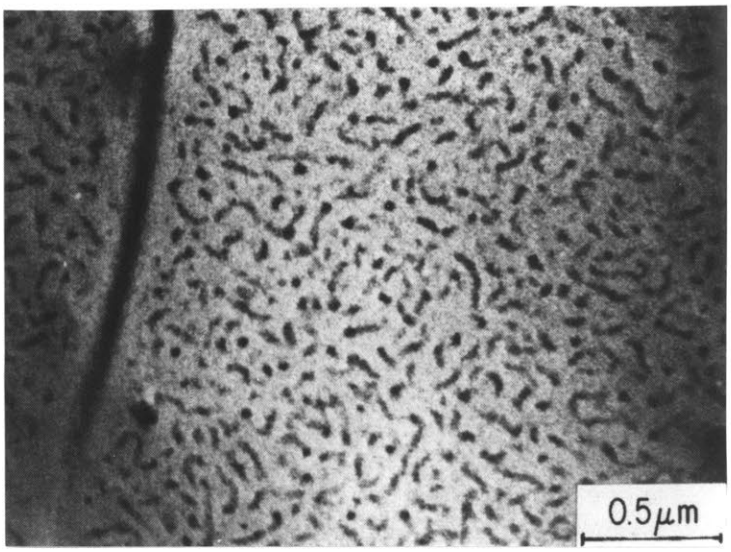

(b)

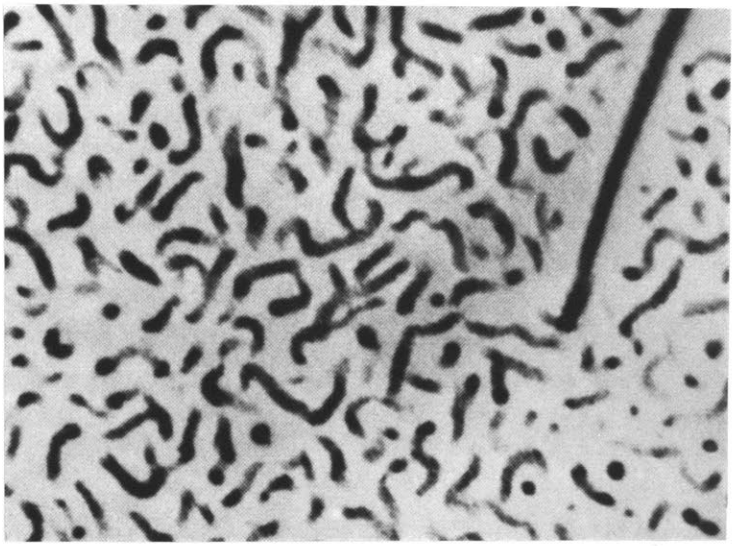

Figure III.3

(200) dark-field micrographs from the Swann, Duff, and Fisher study showing spinodal-like structures developed in an Fe-23.5% Al alloy when a single-phase FeAl specimen is held within the α + FeAl two-phase field for 15 minutes (a) and 2 hours (b).

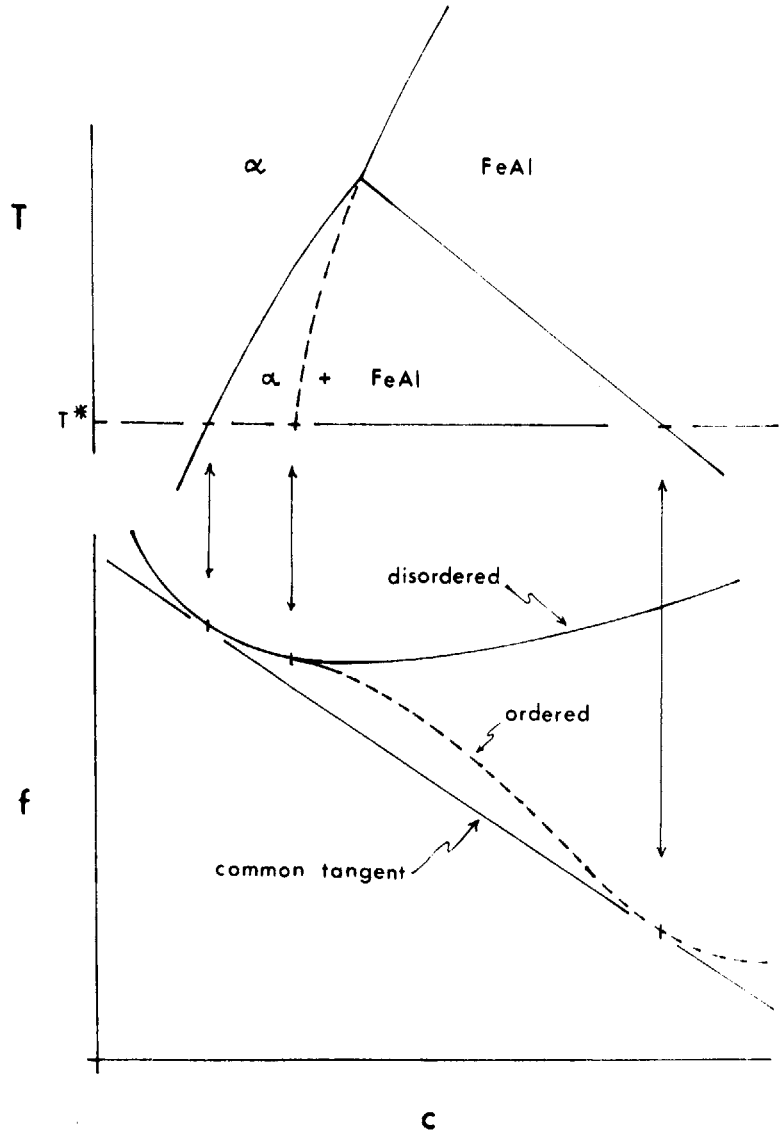

Figure III.4

A schematic representation of the free energy, f, versus composition, c, at temperature T* within the miscibility gap (lower graphs). The related temperature-composition phase diagram is plotted above. A conditional spinodal (not shown) arises in the phase diagram because of the negative curvature region of the ordered free energy.

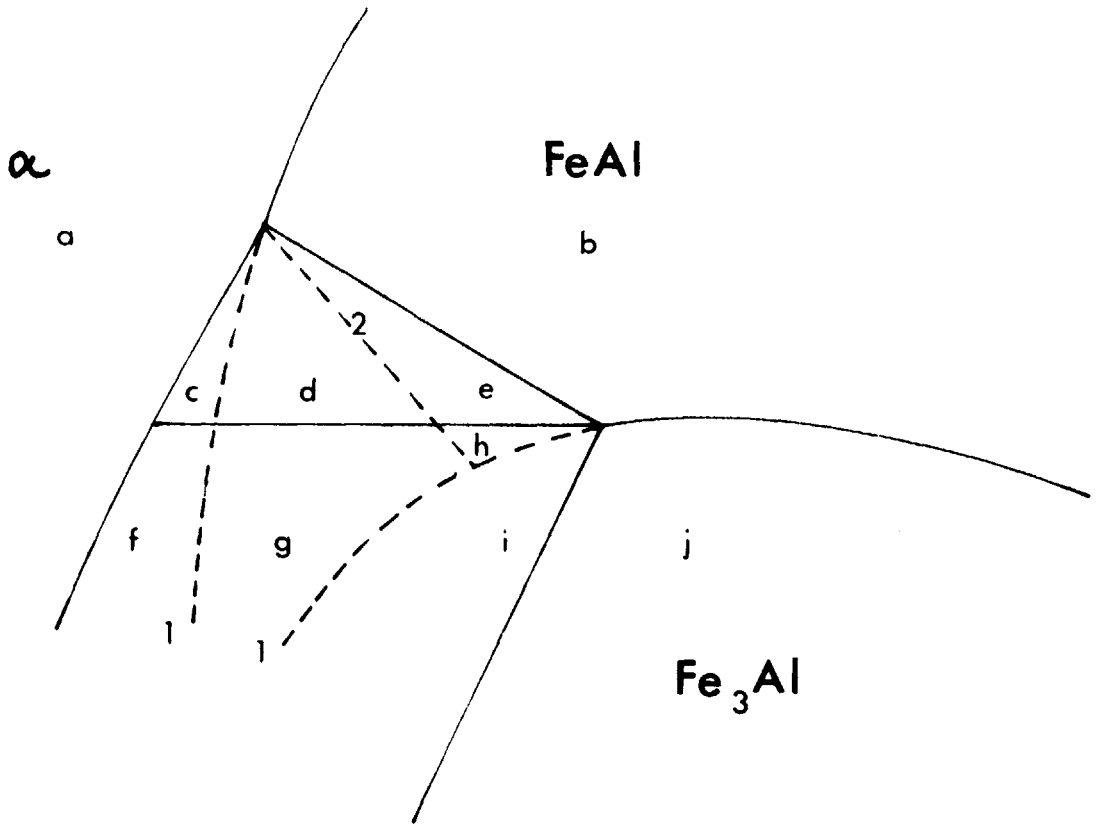

Figure III.5

A schematic indication of metastable continuous ordering lines(1) and conditional spinodal (2) within the miscibility gap of the Fe-Al coherent-phase diagram. The lines partition the diagram into ten areas, labelled a-j, used in the text for classification of transformation mechanisms.

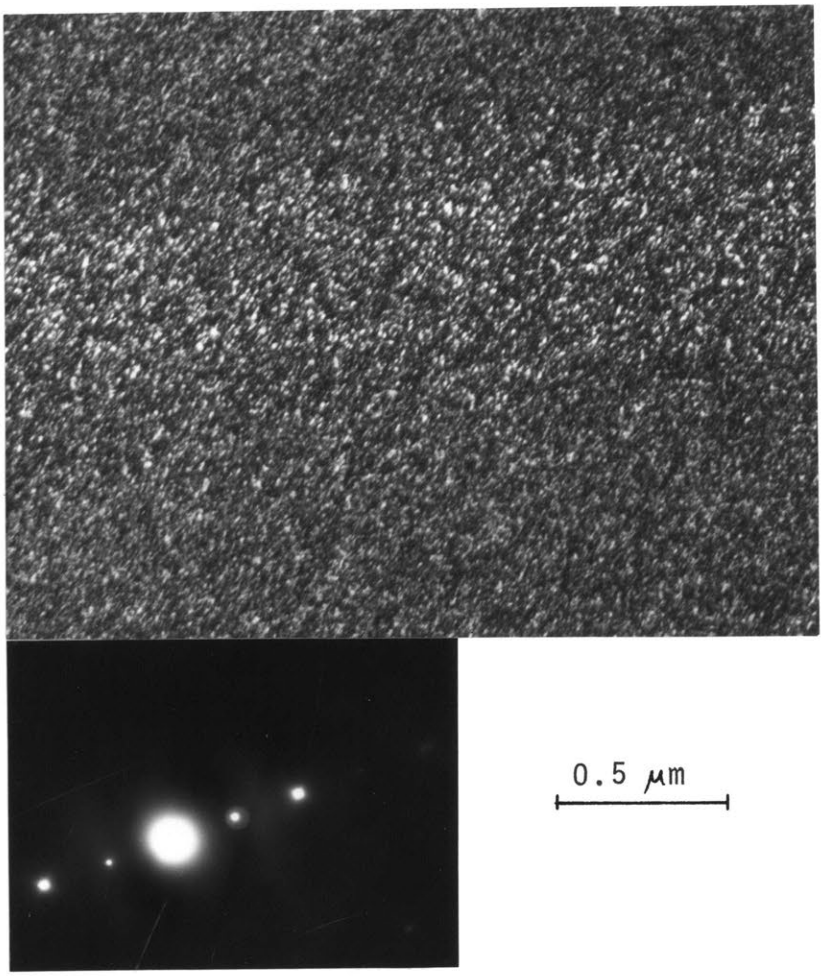

Figure III.6

A (200) dark-field micrograph and selected area diffraction pattern of an Fe-23% Al alloy showing the extent of ordering during a rapid quench from 725°C into cold brine.

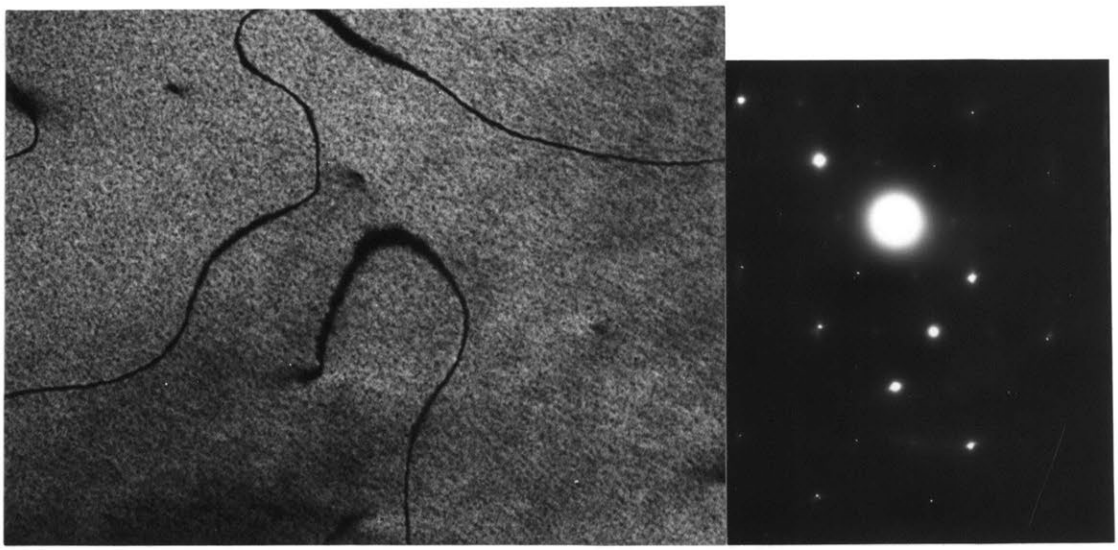

(a) aged 10 seconds 0.5 μm

Figure III.7

A series of dark-field micrographs imaging FeAl superlattice reflections in Fe-24% Al alloy specimens that were initially single-phase FeAl, then decomposed at 570°C for 10 seconds (a), 1 minute (b), and 5 minutes (c), prior to quenching. The resulting microstructures are like that of spinodal decomposition in an isotropic system. The (110) diffraction pattern in (a) shows diffuse Fe_3Al spots resulting from a slow quench. Diffuse intensity near the fundamentals in diffraction patterns (b) and (c) is believed to be due to temperature diffuse scattering.
(cont.)

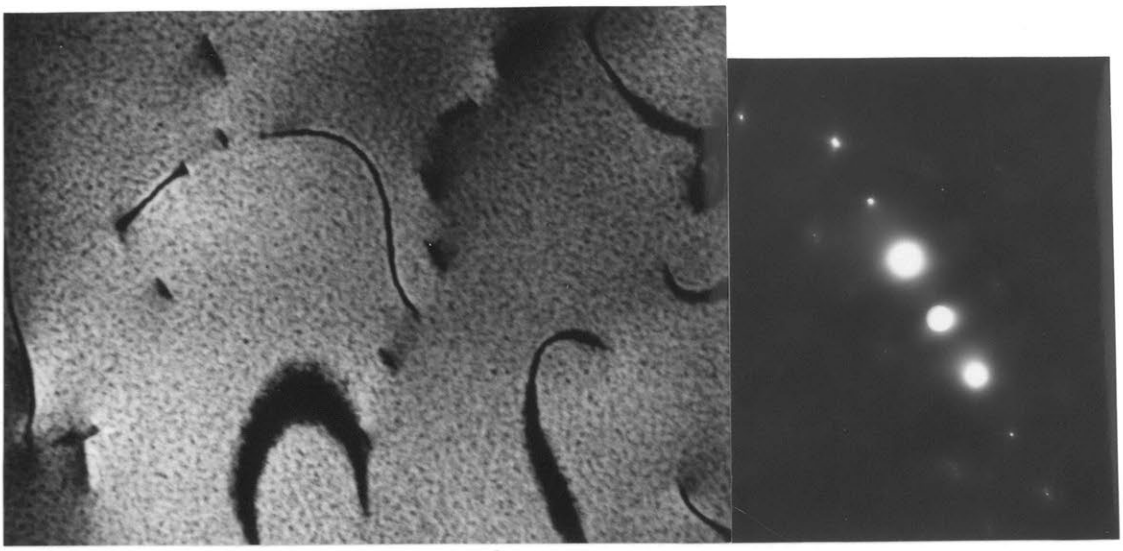

(b) aged 1 minute

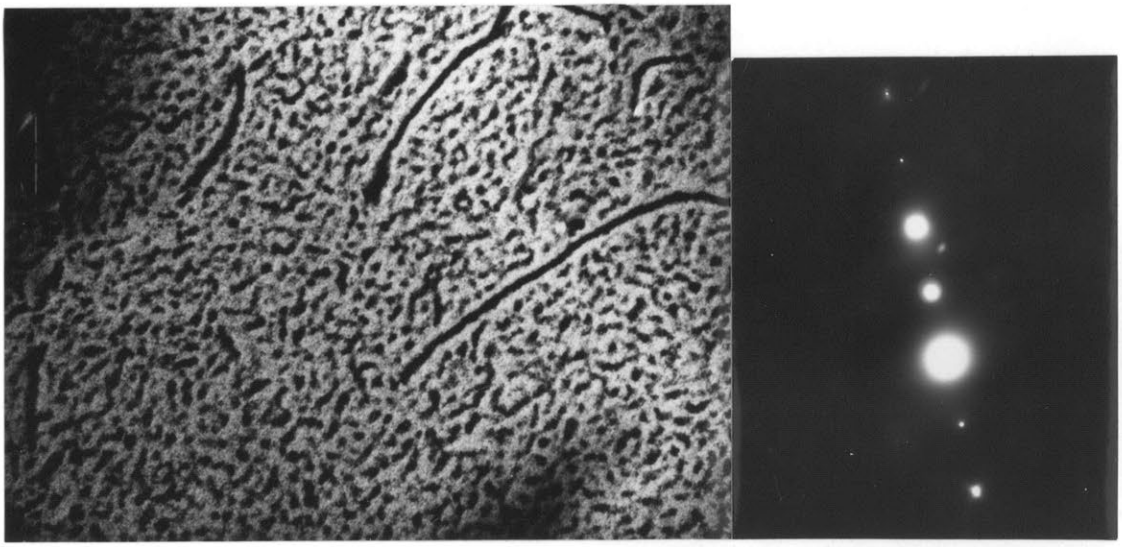

(c) aged 5 minutes

0.5 μm

Figure III.7 continued

(a)

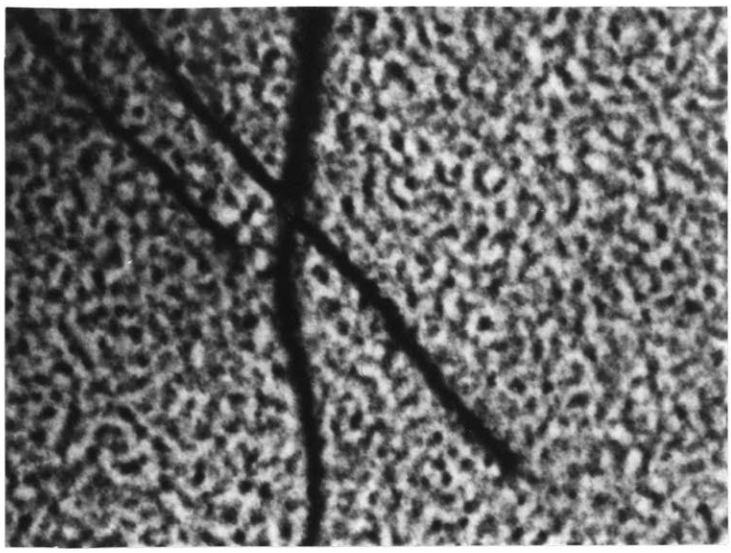

(b)

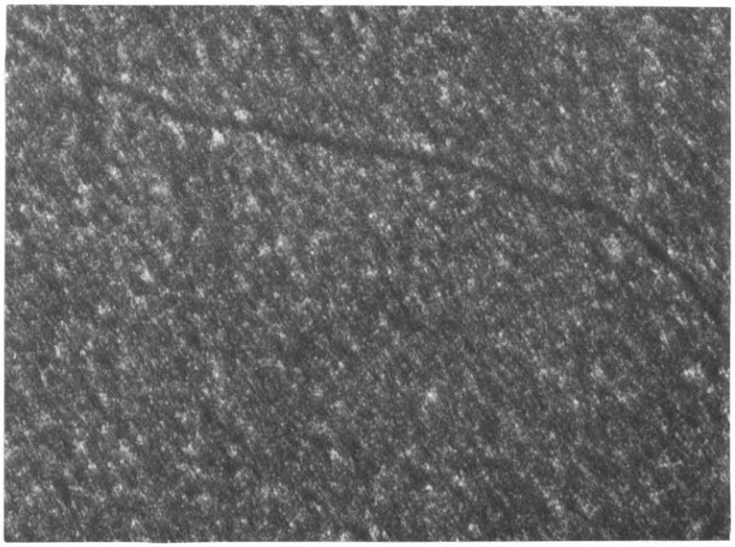

0.2 μm

Figure III.8

Fe-24% Al specimen heat treated 1 hour at 625°C, quenched, then aged 150 seconds at 539°C. (a) shows continuous decomposition of ordered B2; (222) dark-field micrograph. (b) shows a (111) dark-field micrograph of the same specimen, revealing a high density of very fine (∿ 30 Å) domains of the DO_3 phase in the aluminum-rich regions of the specimen. The micrographs are evidence of spinodal decomposition preceding the reordering reaction.

(a)

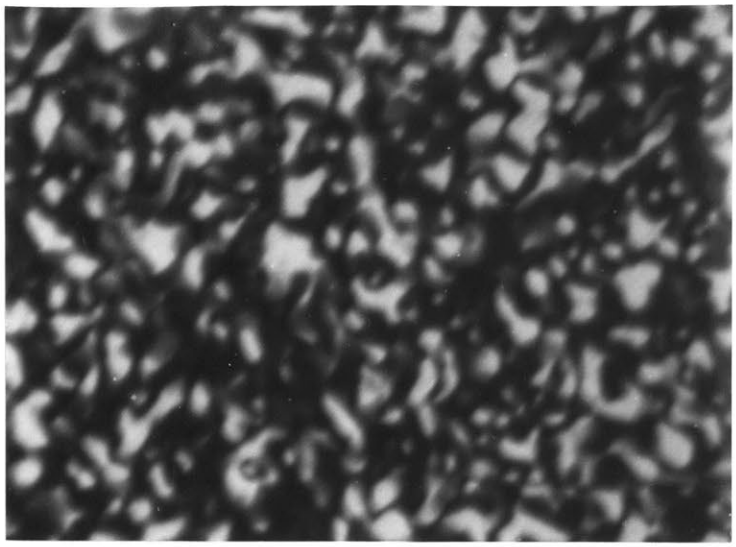

(b)

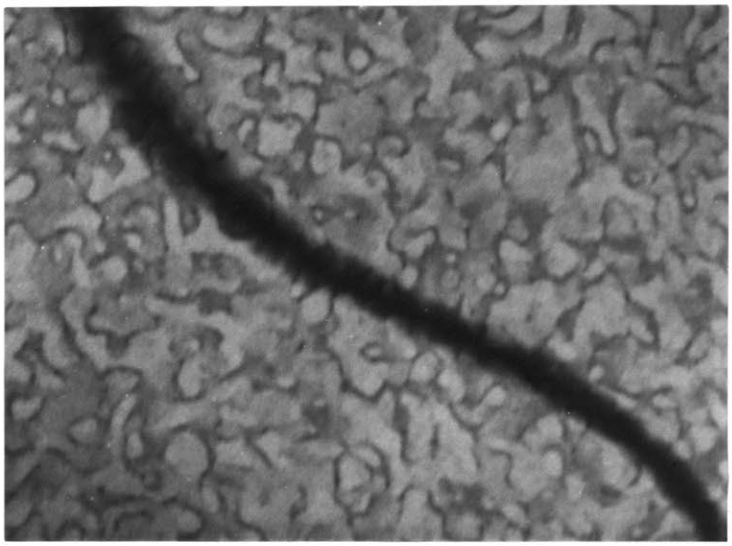

0.2 μm

Figure III.9

Fe-24% Al specimen heat treated 1 hour at 625°C, quenched, then aged 300 seconds at 475°C. (a) shows a (111) dark-field micrograph revealing a high degree of DO_3 order. Much of the dark contrast is due to $a'_o/2$ [100] APB's. (b) shows a (222) dark-field micrograph of the same specimen showing that the $a'_o/2$ [100] APB's are coated with a continuous layer of the disordered phase.

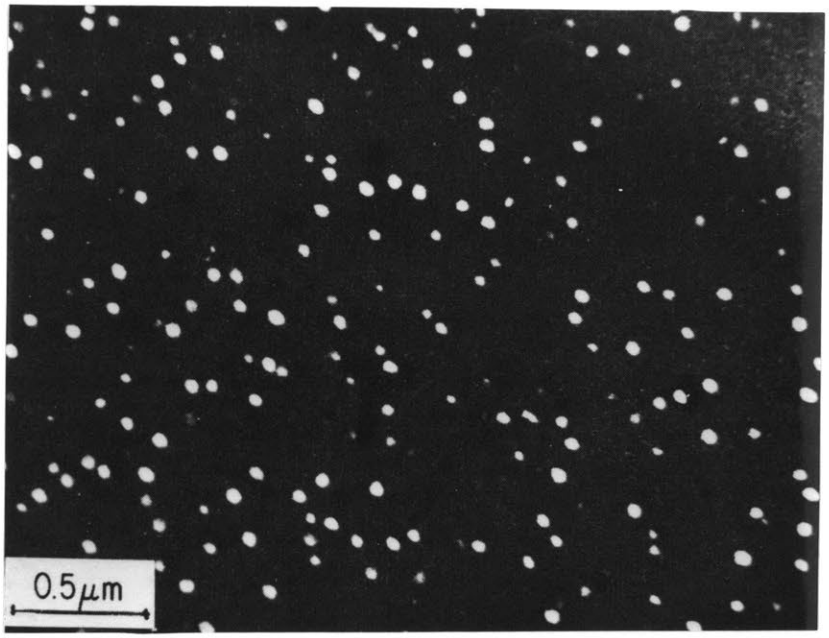

Figure III.10

Initially disordered and quenched Fe-22.7% Al alloy aged for 2 hours at 559°C and quenched. (200) dark-field micrograph shows a dispersion of coherent FeAl particles in a disordered matrix. From Reference 12.

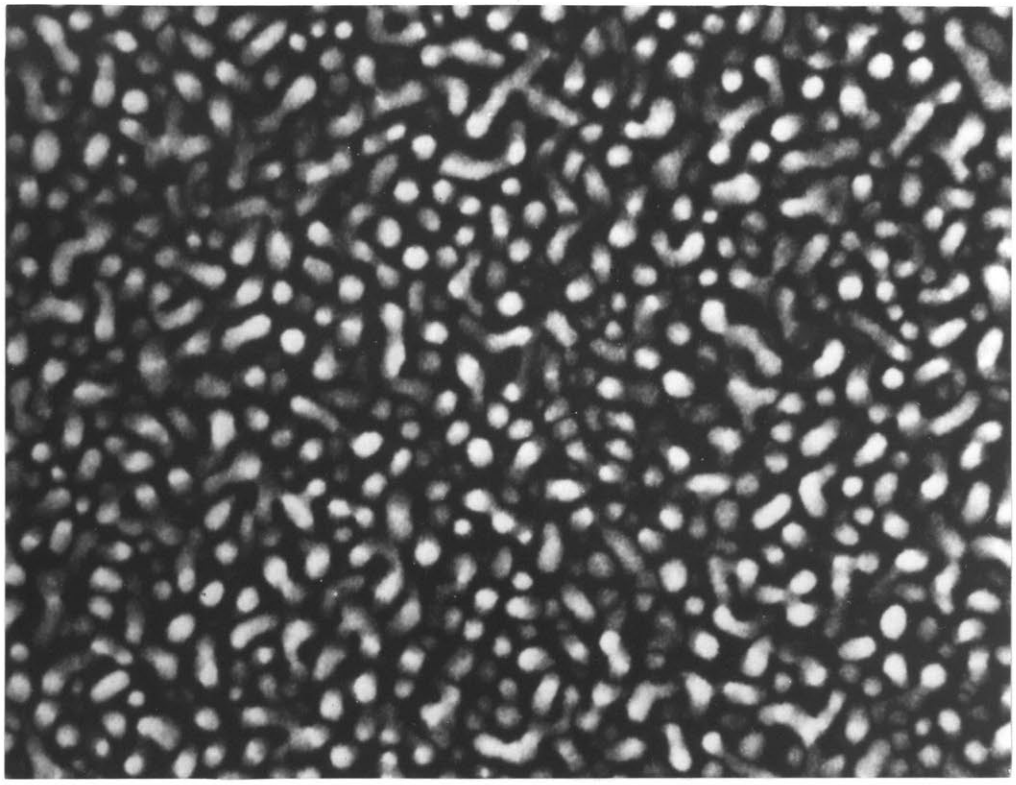

0.5 μm

Figure III.11

Initially disordered and quenched Fe-23% Al alloy aged at 570°C for 160 minutes and quenched. (200) dark-field micrograph shows interconnected FeAl domains resulting from metastable continuous ordering followed by heterogeneous formation of α on APBs.

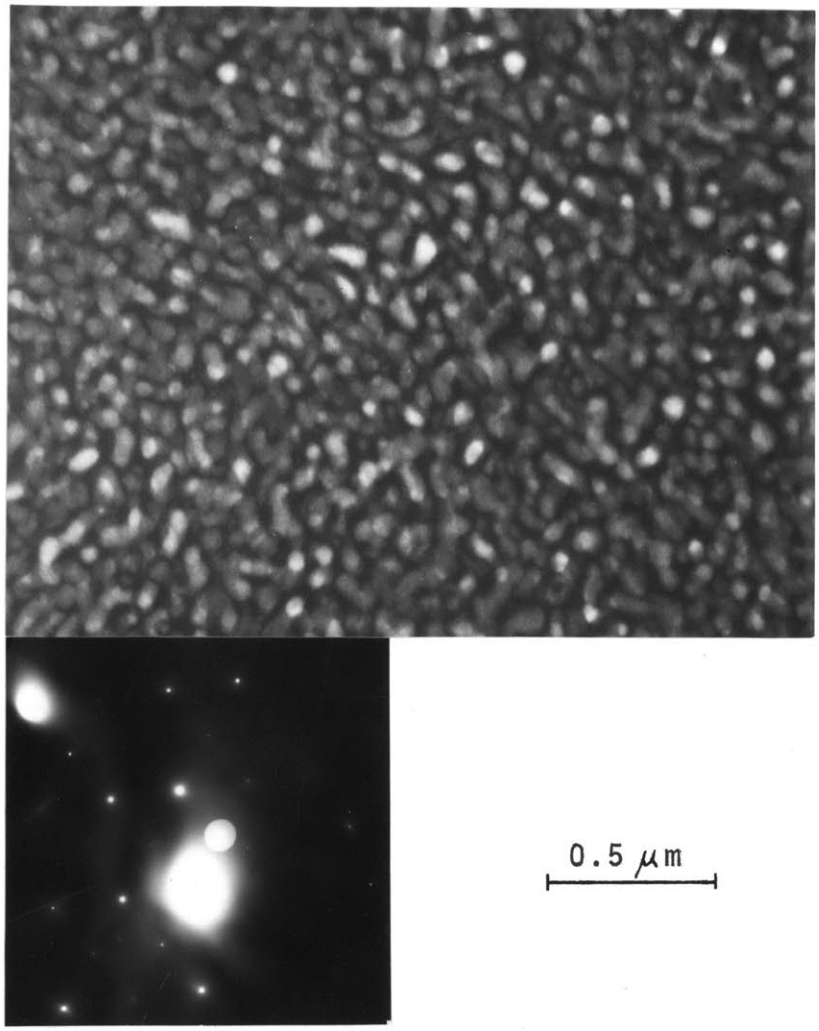

Figure III.12

(111) dark-field micrograph and selected-area diffraction pattern of an Fe-23% Al alloy, initially disordered, quenched, and aged at 530°C for 150 minutes. The microstructure consists of highly-interconnected Fe_3Al regions in a disordered matrix.

(a)

(b)

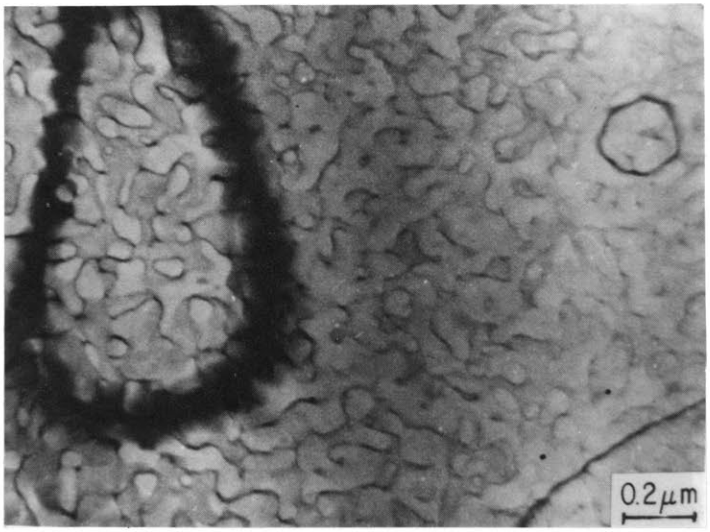

Figure III.13

Initially disordered and quenched Fe-24.1Al alloy aged at 452°C 64 hours and quenched. (a) shows a (111) dark-field micrograph revealing a high degree of DO_3 order. (b) shows a (222) dark-field micrograph demonstrating that a layer of the disordered phase has formed on the $1/2a'_o$ [100] APBs. From Reference 12.

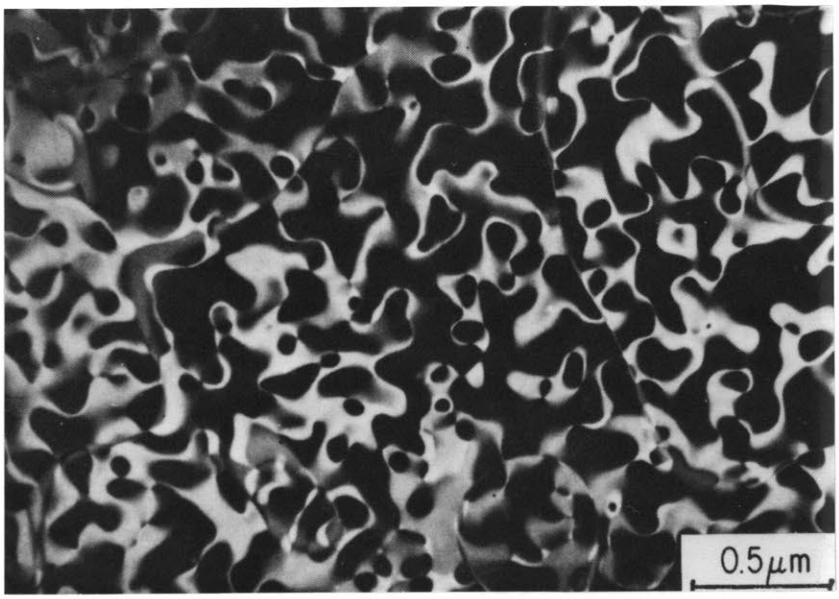

Figure III.14

Fe-25.5% Al aged at 400°C for 40 hours and quenched. (111) dark-field micrograph reveals small $1/2a'_0$ [100] domains within larger $1/4a'_0$ [111] domains indicating that B2 ordering preceeded DO_3. From reference 12.

TABLE III.1

A Summary of the Mechanisms of Decomposition of Single-Phase Iron-Aluminum Alloys within the Miscibility Gap

Initial State → Final State	Location in Fig. III.5	Sequence of Mechanisms	Rules Invoked
$B2 \rightarrow DO_3$	b→j	C.O	1
$B2 \rightarrow \alpha + B2$	b→d	Large Initial B2 domains: S.D.	3
		Small initial B2 domains: segregation of Fe to APBS enhanced by uphill diffusion, forming α on APBS	3,5
	b→c	Large initial B2 domains: Nucleation and growth of coherent α particles within B2 domains and on APBS	4
		Small initial B2 domains: Heterogeneous precipitation of α on APBS	4
$B2 \rightarrow \alpha + DO_3$	b→g	Large initial B2 domains: S.D. followed by $B2 \rightarrow DO_3$ C.O. of Al-rich regions	3,2
		Small initial B2 domains: Segregation of Fe to APBS enhanced by uphill diffusion, forming α at APBS. Then $B2 \rightarrow DO_3$ C.O. of initial domain cores	3,5,2
	b→h + b→i	Large initial B2 domains: Nucleation and growth of coherent α particles within B2 domains and on APBS, then $B2 \rightarrow DO_3$ C.O.	4,2
		Small initial B2 domains: Heterogeneous precipitation of α on APBS followed by $B2 \rightarrow DO_3$ C.O. of initial domain cores.	4,2
		$B2 \rightarrow DO_3$ C.O. followed by segregation of Fe to APBS, forming an α layer on APBS.	2,4

(Cont'd)

Initial State → Final State	Location in Fig. III.5	Sequence of Mechanisms	Rules Invoked
B2	a→b	C.O.	1
$\alpha \rightarrow \alpha + B2$	a→c	Homogeneous nucleation and growth of coherent B2 particles	4
	a→d a→e	Since the reactions involve initial $\alpha \rightarrow B2$ C.O., they proceed according to b→d and b→e reactions for small initial B2 domains	2, then see above
$\alpha \rightarrow \alpha + DO_3$	a→f	Homogeneous nucleation and growth of coherent ordered particles. Initial nucleus may be B2. (see text)	4
	a→g a→h a→i	Since the reactions involve initial $\alpha \rightarrow B2$ C.O., they proceed according to b→g, b→h, and b→i reactions for small initial B2 domains.	2, then see above
$\alpha \rightarrow DO_3$	a→j	Successive C.O. reactions: $\alpha \rightarrow B2$ followed by $B2 \rightarrow DO_3$	1

Key: C.O. = continuous ordering

S.D. = Spinodal decomposition

SUMMARY

1. Two recent phase diagram determinations for the iron-rich iron-aluminum alloys, that of Swann, Duff, and Fisher, and that of Okamoto and Beck, are both correct for this system although they contain significant differences. Transmission electron microscopy and electron diffraction were used to show that the Swann, Duff, and Fisher phase diagram is a coherent metastable one, and that the Okamoto and Beck diagram is the equilibrium incoherent phase diagram.

2. The mechanisms of phase separation that occur when a single phase decomposes within the miscibility gap of a system containing a tricritical point were investigated. A thermodynamic model of Richards and Cahn indicated that such a system should exhibit both continuous ordering and phase separation in addition to discontinuous phase changes. This model and kinetic principles were used to develop a set of rules to distinguish which mechanisms would be observed for specific transitions, along with their sequence if more than one were dictated.

The set of rules was applied to the decomposition of a single phase within the miscibility gap of the iron-rich iron-aluminum alloys. The rules predicted that the decomposition of a specific single phase within a specific two-phase field of the phase diagram should proceed via different

mechanisms and/or sequences, depending on alloy composition and decomposition temperature. Transmission electron microscopy and electron diffraction were used to study the transitions experimentally. The observed microstructures were in excellent agreement with the predicted mechanisms.

SUGGESTIONS FOR FURTHER WORK

The following points, which have arisen from the results of this thesis investigation, should be persued further.

1. The necessary measurements to determine strains in coherent two-phase microstructures that are observed in the Fe-Al system should be made, and these correlated with the temperature-depression of the tricritical point in the coherent phase diagram.

2. The microstructures that develop within the conditional spinodal need to be characterized further in an attempt to determine whether or not existing theories of spinodal decomposition apply within the miscibility gap of this system. In particular, it should be determined if the microstructures have a characteristic wavelength; if so, its time variation and orientation dependence should be carefully examined. Transmission electron microscopy, coupled with optical fourier transforms of the microstructures, could be useful in this determination.

3. The detailed microstructural changes in the early stages of continuous ordering transformations are still unknown for the iron-aluminum system. The FeAl $\rightarrow$ Fe_3Al transition would be a natural one to study as the Fe_3Al ordering can be supressed nearly completely by quenching. A study of

the early stages of the non-equilibrium ordering reaction at high undercoolings may elucidate the role of vacancies in the continuous growth of ordering waves.

4. Many aspects of the behavior of antiphase boundaries in this system need further study. One area is to determine the conditions under which the two types of APBs are wetted by the disordered phase. A more fundamental study could be made of APB mobility; in this system APBs can be produced by deformation and therefore the disjunction of artificially produced intersections would be studied in a system where the APB energies are easily varied.

5. High resolution electron microscopy techniques should be carefully applied to study the exact nature of the critical fluctuations that can be quenched-in these alloys. In particular, it would be interesting to see if fluctuation in long-range order could be distinguished from those in composition. Distinct differences should be observed in the character of the fluctuations close to, and away from the tricritical point.

BIOGRAPHICAL NOTE

The author was born in Washington, D. C. on July 1, 1948. A year later he was moved to Cannondale, Connecticut where he grew up on an old farm. He attended public schools in Wilton, Connecticut, graduating from Wilton High School in 1966.

As an undergraduate he attended Stevens Institute of Technology in Hoboken, New Jersey, where he graduated with honor in 1970.

On entering M.I.T. in September, 1970, he was awarded an Allegheny Ludlum Steel Corporation Fellowship, which he held for two years. He obtained a Master of Science degree in metallurgy in September, 1971, with John Cahn as his advisor. In his third year at M.I.T. he was employed as a teaching assistant, working for Professors Wulff, Russell, Witt, and Coble.

During the summers, and in his final year, he was a research assistant to John Cahn. The author is presently an instructor in the Department of Materials Science and Engineering at M.I.T.

Publications:

1. S.M. Allen and J.W. Cahn, "Ground State Structures in Ordered Binary Alloys with Second Neighbor Interactions," Acta Met. 20, 423(1972).

2. S.M. Allen and J.W. Cahn, "A Correction to the Ground State of FCC Binary Ordered Alloys with First and Second Neighbor Pairwise Interactions," Scripta Met. 7, 1261(1973).